Masters Theses   Student Theses and Dissertations

Summer 2007

Synthesis, characterization and application of Pd-Pt bimetallic nanoparticles and carbon nanotubes supported nanocomposites

Guoqiang Ren

Follow this and additional works at: https://scholarsmine.mst.edu/masters_theses

Part of the Chemical Engineering Commons

Department:

Recommended Citation

SYNTHESIS, CHARACTERIZATION AND APPLICATION OF Pd-Pt BIMETALLIC
NANOPARTICLES AND CARBON NANOTUBES SUPPORTED
NANOCOMPOSITES

by

GUOQIANG REN

A THESIS

Presented to the Faculty of the Graduate School of the

UNIVERSITY OF MISSOURI-ROLLA

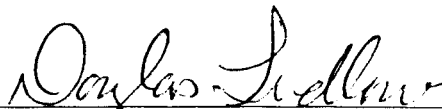In Partial Fulfillment of the Requirements for the Degree

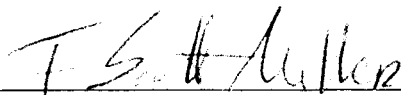MASTER OF SCIENCE IN CHEMICAL ENGINEERING

2007

Approved by

_____
Yangchuan Xing, Advisor

_____
Douglas K. Ludlow

_____
F. Scott Miller

ABSTRACT

A study on the synthesis of Pd-Pt alloy nanoparticles and composition evolution of the alloys was reported. The synthesis followed a hot organometallic route, with Pd and Pt acetylacetonate as the metal precursors and trioctylphosphine as the solvent. The size of the Pd-Pt nanoparticles narrowed down with time and reached a final size of 3.5 nm in about 10 min. The alloy compositions evolved with time and reached the preset Pd to Pt ratio of precursors in 120 min. An atomic exchange process between the Pt-TOP complex and the Pd atoms at the nanoparticle surface was proposed to elucidate this synthesis process.

Temperature-induced restructuring of the Pd-Pt superlattices was investigated and an irreversible phase transition from an ordered state to a disordered state was observed when the Pd-Pt nanoparticle superlattices were heat treated at temperatures ranging from 100 to 110 °C. The superlattices formed at room temperature showed distorted hexagon structures but they became better-ordered when treated at a proper temperature.

Demonstrated with Pd-Pt and CoPt$_3$ nanoparticles, a novel technique that involves fast evaporation of a suspension containing sonochemically-treated carbon nanotubes (CNTs) and the metal nanoparticles was developed for deposition of colloidal metal nanoparticles on the CNTs. This technique seems to be applicable for the deposition of other nanoparticles as well, since it involves only a physical process and has the advantages that the nanoparticle size and number density on the CNTs can be independently controlled, opening ways of producing tailored nanomaterials.

ACKNOWLEDGMENTS

The author would like to sincerely express his gratitude to his advisor, Dr. Yangchuan Xing, for his guidance, assistance and financial support during the completion of the work. The author would also like to thank Dr. Douglas K. Ludlow and Dr. F. Scott Miller for their instructions in the graduate level courses and for serving on the graduate committee. Thanks also to other graduate students in the group for their help.

The support from the Department of Chemical & Biological Engineering in the University of Missouri – Rolla is greatly acknowledged.

Finally, the author would gratefully thank his family for their understanding and support in pursing his graduate degree.

TABLE OF CONTENTS

LIST OF ILLUSTRATIONS

PAPER I

SYNTHESIS AND COMPOSITION EVOLUTION OF BIMETALLIC Pd-Pt ALLOY NANOPARTICLES

Guoqiang Ren[1], Honglan Shi[2] and Yangchuan Xing[1,2]

[1]Department of Chemical & Biological Engineering
[2]Environmental Research Center for Emerging Contaminants
University of Missouri – Rolla
Rolla, MO 65409, USA

Email: xingy@umr.edu

Abstract

This paper reports a study on the synthesis of Pd-Pt alloy nanoparticles and composition evolution of the alloys. The synthesis involves Pd and Pt acetylacetonate as the metal precursors and trioctylphosphine (TOP) as the solvent. Thermal decomposition of the Pd-TOP complex resulted in Pd nanoparticles, while substitution of Pt in the Pt-TOP complex by Pd allowed formation of the Pd-Pt alloys. It was observed that the Pd-Pt nanoparticles formed at the very beginning in the synthesis process are Pd rich with various nanoparticle sizes ranging from 1.5 to 25 nm in diameter. These nanoparticles averaged out through a digestive ripening process and reached a final size of 3.5 nm in about 10 min. The alloy compositions evolved throughout the synthesis process and only reached the preset Pd to Pt ratio of the precursors in 120 min. It was found that Pt acetylacetonate alone in TOP cannot produce Pt nanoparticles, which was attributed to the formation of a Pt-TOP complex and a strong coordination of Pt to the phosphine. This observation led us to propose an atomic exchange process between the Pt-TOP complex and the Pd atoms at the nanoparticle surface. As a result, the alloy formation process is

limited by a substitution and diffusion rate of the Pt atoms at the surface of the alloy nanoparticles.

1. Introduction

Platinum and palladium are known catalysts for many chemical processes. They have been extensively studied for various applications, including electrocatalysis [1-3], hydrogenation [4-11], and oxidation of organic compounds [12-14]. Nanoparticles of such metals with a high surface to volume ratio and a large portion of active surface atoms are of particular interest due to that these properties can be manipulated in a desirable way. Furthermore, alloys of the metals are of particular interest as they would provide a combination of benefits from the individual elements.

The synthesis of Pd-Pt nanoparticles by reduction of metal precursors in an aqueous phase has been studied and reported in recent years. Preparation of colloidal Pd-Pt nanoparticles from non-ionic microemulsions was reported by Touroude et $al.$ [15], who reduced metal salts (H_2PtCl_6, and $PdCl_2$) using hydrazine hydrate in a water-in-hexadecane microemulsion stabilized by pentaethylene glycol dodecyl ether. Aggregated Pd-Pt nanoparticles ranged from 10-100 nm (Pt to Pd atomic ratio is 35:65) and single particles of 2-5 nm (96:4) were synthesized in that process. Solla-Gullon et $al.$ [16] applied a similar microemulsion technique and obtained surfactant-capped nanoparticles with Pt:Pd ratio from 4:1 to 1:4. Wu et $al.$ [17] used water/AOT/isooctane microemulsions and obtained 7-10 nm Pd-Pt nanoparticles, with Pt:Pd ratios from 1:9 to 9:1. Veiz et $al.$ [18] synthesized Pd-Pt nanoparticles in a colloidal solution in which excessive $NaBH_4$ was used to reduce K_2PdCl_4 and K_2PtCl_4 precursors with various molar

ratios in the presence of a cationic surfactant. Their results showed that the sizes of the bimetallic Pd-Pt nanoparticles ranged from 4 to 6 nm, with Pt:Pd ratios of 1:4, 1:1 and 4:1. Recently, Adlim *et al.* [19] reported chitosan-stabilized Pd-Pt nanoparticles with 2-20 nm in diameter.

In this paper, we report a new method that we have been developing for the synthesis of monodisperse Pd-Pt nanoparticles in organic solvents. By using an organometallic process, we have synthesized Pd-Pt nanoparticles featuring both small nanoparticles (~3.5 nm) and monodispersed sizes. The compositions of the nanoparticles can be controlled not only by ratios of the metal precursors but also by the aging time, while the sizes of these nanoparticles remain unchanged. The technique provides a new way to synthesize Pd-Pt nanoparticles with composition and size controlled properties.

2. Experimental Methods

2.1 Synthesis of Pd-Pt bimetallic nanoparticles

Pd-Pt nanoparticles were synthesized using an organometallic process. Platinum acetylacetonate ($Pt(acac)_2$) and palladium acetylacetonate ($Pd(acac)_2$) were used as precursors in trioctylphosphine (TOP) with 1-adamantanecarboxylic acid (ACA) and 1-hexadecylamine (HDA) as surfactants for the synthesis. A Pt precursor mixture was prepared by dissolving 11.90 mg (0.030 mmol) of $Pt(acac)_2$ (Alfa Aesar) and (46.5 mg) 1,2-hexadecanediol (90%, Sigma-Aldrich) into 5 mL TOP. 29.7 mg 1-admantanecarboxylic acid (ACA, 99% Sigma-Aldrich) and 7.4 mg 1-hexadecylamine (HDA, 90%, Sigma-Aldrich) were also added as surfactants and co-surfactants [20]. This mixture was heated to 60°C and dispersed in an ultrasonic water bath until a clear yellow

solution was formed. A Pd precursor mixture was prepared by adding 9.3 mg (0.031 mmol) Pd(acac)$_2$ (from Alfa Aesar) into 2.0 ml trioctylphosphine (TOP, 90% purity from Sigma-Aldrich) of which the solution was heated to 60°C until a clear homogeneous orange solution was formed, indicative of the formation of a Pd-TOP complex [21].

After the preparation of each precursor mixture solution separately, the two mixture solutions were added into a three-neck flask in which 4 mL TOP was also added. This organic solution was stirred using a Vortex mixer (Vortex Gene 2, Scientific Industries) for 5 min until a homogeneous solution was formed. The solution was heated to 300°C and it turned black in a minute. The solution was then refluxed at that temperature for different time durations. The nanoparticles were precipitated by adding 20 mL ethanol to the solution. The precipitate was washed and separated again in a centrifuge (Centra CL 2.0, Thermo IEC) with ethanol for four times. The final precipitate can be easily redispersed in nonpolar hexane or toluene.

To track the changes of alloy compositions in the Pd-Pt nanoparticles, a reaction mixture with double amount of the materials was used. This allowed continuous sampling at different time durations for analysis of the alloy compositions. The reaction mixture was sampled using a syringe with 1.25 mL each at a time for the following time durations: 3, 5, 10, 30, 40, 60, 120, 240, 480 and 660 min. For each sampling, the sample was injected into a Pyrex glass vial and 10 mL ethanol was added to cool it for handling. Each sample was washed with ethanol for three times and a black precipitate was obtained for examination.

2.2 Characterization of Pd-Pt nanoparticles

Size and shape characterizations of the Pd-Pt nanoparticles were achieved on a transmission electron microscope (TEM) (EM 430, Philips) operating at 300kV. The TEM specimen was prepared by dispersing a small amount of Pd-Pt in hexane under sonication. A drop of the dispersion was transferred with a pipet and put on a TEM grid (400-mesh carbon-coated copper grid, Electron Microscopy Sciences), rapidly drying under open atmosphere with the evaporation of hexane. The grid was then examined with the TEM and images were taken. To obtain size information, measurement of ~500 nanoparticles was made with image analysis software (Scion, NIST) and a statistical result of the size was obtained. Energy Dispersive X-ray Spectrum (EDS, Noran Voyager III light element EDS system) analysis of the specimen was also performed to determine elemental compositions. To enhance the signal detection, the TEM sample holder was tilted 20° towards the EDS detector during data acquisition.

The crystalline structures of Pd-Pt nanoparticles were determined by powder X-ray diffraction. The computerized Scintag 2000 diffractometer was equipped with Ni-filtered Cu Kα (λ=0.15406 nm) X-ray source and a Theta-Theta XDS 2000 goniometer with a solid state Ge detector and a fixed slit. To prepare samples for X-ray diffraction (XRD), the as-prepared Pd-Pt nanoparticles were mixed with ~5 mg of carbon black/hexane slurry and dried in a vacuum furnace at 70 ^{o}C. The dried powders were pressed onto a double-sided Scotch tape on a glass slide. Scanning of the sample was performed at 0.030^{o}/min to ensure detailed structure acquisition.

The compositional information of the Pd-Pt nanoparticles was obtained by Inductively Coupled Plasma Mass Spectroscopy (ICP-MS) analysis. After the

synthesized Pd-Pt nanoparticles were washed 3 times with 20 mL of ethanol to ensure that unreacted precursors were removed, a portion of the sample was transferred to a Pyrex glass vial. 3 mL of Aqua Regia (HNO_3:HCl at 1:3 volumetric ratio) was added to the vial containing the Pd-Pt nanoparticles. The digestions was proceeded by heating the sealed vial in a 60°C ultrasonic water bath for 2 h, followed by 7 mL de-ionized water addition and 4 h heating with the vial uncovered. The as-obtained aqueous solution was diluted to 50 mL with de-ionized water. Pd and Pt in the sample were then detected by ICP-MS with further appropriate dilutions. An Elan DRCe ICP-MS instrument (SCIEX, PerkineElmer) equipped with a cross-flow nebulizer and nickel cones was used for analysis. The RF power was 1400 kW. Argon flow rates for the plasma and auxiliary gas were 15 and 1.0 L/min, respectively. Samples were delivered at 1.0 mL/min by a peristaltic pump. Quantitation was performed at m/z 195 for Pt and 106 for Pd. The standard stock solutions for calibration were purchased from PerkinElmer. The initial instrument calibration was carried out at the concentration of 0.1-500ppb linear range. Internal standard In was used for Pt and Ho was used for Pd detection. These standards were added continuously online as a mixture.

Oxidation states of the alloy nanoparticles were analyzed with X-ray photoelectron spectroscopy (XPS) (Axis 165, Kratos). The spectrometer is equipped with a concentric hemispherical analyzer (CHA) which uses 8 channeltron detectors. The sample was ion sputtered with a differential ion gun for 60 seconds at 4 kV. A Mg Kα anode, operated at 15kV and 225 W with a photon energy of hv = 1253.6 eV, was used as the X-ray source. The base pressure of the chamber during inspection was 10^{-9} Torr. The pass energy was 80 eV during the survey scan and 20 eV for the windows scan.

3. Results and Discussion

3.1 Characterization of Pd-Pt nanoparticles

Figure 1 shows a typical TEM image of the Pd-Pt nanoparticles synthesized with heating for 40 min and cooling at ambient. It can be seen that the nanoparticles are monodisperse and uniform with a spherical shape. The size of the Pd-Pt nanoparticles measured from the TEM images was as 3.5 ± 0.3 nm in diameter. EDS spectra showed the samples contain both Pt and Pd elements.

The long-range order structure of the nanoparticles revealed by XRD is shown in Figure 2. The broad peak near the position $2\theta=25°$ was due to the carbon support. Both of the reflection peaks from Pt and Pd with a face-centered cubic (fcc) structure were indexed with Miller indices in the XRD pattern. The 2θ values of 39.75, 46.24, 67.44, 81.28 (for Pt, JCPDS 04-0802) and 40.11, 46.65, 68.11, 82.09 (for Pd, JCPDS 46-1043) correspond to (111), (200), (220) and (311) crystal planes for each pure metal, respectively. For their alloys, the intensity patterns of the reflections are similar to that reported for Pd-Pt nanoparticles on different supports [12, 22]. The particle size calculated from the XRD measurements based on line broadening of the Pt(111) reflection was ~3.6 nm using the Scherrer formula, which matches quite well with that from the TEM analysis, indicative of that the Pd-Pt nanoparticles are single grains.

Morphological evolution of the Pd-Pt nanoparticles during the synthesis was examined at different time durations. At 3 min (Figure 4a), the nanoparticles had already formed a near spherical shape through homogeneous nucleation with a wide range of sizes, the biggest at ~25 nm and the smallest at ~1.5 nm. However, as time passed, the nanoparticles quickly narrowed down to a smaller size range. At 5 min (Figure 4b), the

size distribution was seen to narrow significantly and at 10 min monodisperse nanoparticles were already achieved with a size of 3.5 ± 0.5 nm and a spherical morphology. Thereafter (up to 480 min), no obvious changes in morphology of the Pd-Pt nanoparticles were observed (Figures 4c and 4d). However, with longer synthesis time durations (> 60 min), we experienced a difficulty in washing the nanoparticles. They have to be washed extensively for re-dispersion.

The change in size with time of the Pd-Pt nanoparticles may be explained with digestive ripening suggested by Lin et al. [23], who observed that nanoparticles capped by surfactants tend to form small uniform nanoparticles at the expense of the larger ones, in contrast to the Oswald ripening. It was observed that phosphines are good digestive agents, which were used for Pt-Fe and Pt-Co alloy nanoparticles [24]. We believe that in our experiment the TOP acted both as a solvent and a co-capping agent to ACA. At the beginning of the synthesis process, Pd nanoparticles were quickly formed from thermal decomposition of the Pd-TOP complex [21], but with a broad size distribution due to fast coagulation. Once the nanoparticles are formed, the surfactants start to cap them. Therefore, at the early stage, the nanoparticle nucleation and growth processes are believed to be much faster than the capping process. With time the interaction of the TOP and the nanoparticles led to digestive ripening, which narrowed the nanoparticles down to a smaller size range by averaging them out until a thermodynamically stable size was reached.

The surface oxidation state of the final Pd-Pt nanoparticles was studied by XPS. For the measurements, the nanoparticles were supported on carbon. The characteristic peaks for each element, Pt_{4f}, Pd_{3d}, O_{1s} and the characteristic elements in the surfactants and

solvents (N in oleylamine, P in TOP) were monitored. The negligible peaks for N and P

evidenced the infinitesimal amount of residual reactants, indicating that the washing

procedures were effective. The XPS also showed that there were negligible metal oxides

in the samples, confirming that the nanoparticles are in metallic states. Details of the XPS

windows scan (Figure 3) showed the peak positions for Pt_{4f} 5/2, 7/2 (a) and Pd_{3d} 3/2, 5/2,

corresponding well with those reported by other workers [17].

3.2 Composition evolution of Pd-Pt nanoparticle alloys

The elemental composition evolution with reaction time is determined by ICP-MS

analysis. The residual organic compounds were digested and the metallic nanoparticles

were dissolved in the Aqua Regia; only the Pt and Pd elements were analyzed. The

overall content of Pd in the nanoparticles, noted by the Pd:Pt atomic ratio, decreases with

time during the synthesis process, from near 3.2 at 5 min to 0.94 at 10 min (Figure 5); the

feeding ratio of the two precursors was 0.95. Therefore, the alloys formed can basically

reach their preset compositions if given enough time. We initially attributed the large

difference in the Pd to Pt ratios to the faster reaction of the Pd-TOP complex leading to

Pd than that of the reduction of the Pt precursor with 1,2-hexadecanediol leading to Pt.

However, when we conducted an experiment on how fast the Pt nanoparticles can be

formed by using just the Pt precursors, we found that Pt nanoparticles cannot be

synthesized alone in this organometallic process even with 1,2-hexadecanediol, a

reductant used in studies by other workers [20]. Further experiments confirmed that 1,2-

hexadecanediol is not necessary since the Pd-Pt alloy nanoparticles can be synthesized

without using any diols. With this information we suspect that, due to the strong

coordination of Pt to the phosphine and a large excess of TOP as a solvent, the Pt-TOP complex can not be decomposed nor reduced. We noted that previous studies have shown that Pt nanoparticles can only be produced with excess oleic acid [25-26].

Therefore, the formation process for the Pd-Pt alloy nanoparticles was believed to be a process of Pd nanoparticle formation with a substitution reaction between Pd and the Pt-TOP complex at the nanoparticle surface, which can be expressed as:

$$(Pd)_n - Pd + Pt - TOP \rightarrow (Pd)_n - Pt + Pd - TOP \tag{1}$$
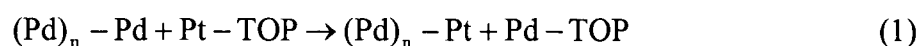
Alloys were formed by diffusion of the Pt into the Pd nanoparticles:

$$(Pd)_n - Pt \rightarrow Pd_n Pt \tag{2}$$

where n is the number of Pd atoms in the nanoparticle. As more and more Pt was substituted, an alloy formulation can be expressed as $Pd_n Pt_m$, where m is the number of Pt atoms in the alloy. At the very beginning of synthesis, n $\gg$ m, but the ratio n:m approached the preset ratio of the precursors over time.

The atomic radii for Pt and Pd are very close at 0.139 nm and 0.137 nm, respectively. Both metals take fcc structure. If a Pt atom forms on a Pd-Pt alloy nanoparticle, it would diffuse into the inside of the Pd nanoparticle without energy barriers, considering that the process occurred at relatively high temperatures. However, since Pt binds to the molecular complex stronger than Pd, exchange of Pt and Pd would be an activated process, and at a given temperature only more time will allow more Pt to form alloys with Pd. We have noticed that although the size of the nanoparticles reached the final size in 10 min, the Pd:Pt ratio did not until about 120 min. A comparison of the radius data of the two metal atoms may justify the fact that changing compositions may not result in changing the nanoparticle size. On the other hand, the longer time that it took

to reach the preset alloy composition indicates that the substitution and diffusion process for the Pt is the slowest among those processes of Pd formation, coagulation, and digestive ripening.

The change of the elemental evolution in alloy Pd-Pt nanoparticles shown in Figure 5 can be fitted with a second order-exponential decay curve, which can be viewed as an overall rate equation for the formation of Pd-Pt alloys under the experimental conditions. The rate should at least represent the substitution and diffusion of the Pt. More definitive study is needed to elucidate the kinetics of the alloy formation.

4. Conclusions

In summary, an organometallic process was developed for the synthesis of Pd-Pt nanoparticles. Small, monodispersed Pd-Pt alloy nanoparticles were successfully synthesized using the process. The Pd-Pt alloy nanoparticles were characterized by TEM, EDS, XRD and XPS for their morphology and by ICP-MS for compositional evolution. A morphological evolution of the alloy nanoparticles was observed, of which the nanoparticles initially formed were of different sizes with near spherical shapes. The alloy nanoparticles eventually became spherical and with a final size of 3.5 nm. Size reduction and narrowing during the synthesis was attributed to digestive ripening. The compositions of the Pd-Pt nanoparticles were found to change over a 120 min period with Pd to Pt atomic ratios from 3.2 to 0.94. This compositional evolution is explained by a kinetic process in which Pd atoms on a nanoparticles substitute Pt form the Pt-TOP complex and the Pt atoms diffuse into inside to form alloys. It was also found that $Pt(acac)_2$ can not be reduced by diols in TOP solvent, which was attributed to the strong

coordination of Pt to the TOP, forming a relatively stable Pt-TOP complex under the experimental conditions. Only when this complex interacts with the Pd nanoparticles, can the Pt be substituted out at the surface of the nanoparticles and further diffuse inside to form the Pd-Pt alloys. It was concluded that the alloy formation rate was limited by the substitution and diffusion rate of Pt. This new technique for the synthesis of Pd-Pt alloy nanoparticles provides an alternative and better way to manipulate nanoparticle properties of both sizes and compositions.

5. Acknowledgement

References

[1]   Papageorgopoulos D C, Keijzer M, Veldhuis J B J and de Bruijn F A 2002 *J. Electrochem. Soc.* **149** A1400-4

[2]   Li X and Hsing I M 2006 *Electrochim. Acta* **51** 3477-83

[3]   Jayashree R S, Spendelow J S, Yeom J, Rastogi C, Shannon M A and Kenis P J A 2005 *Electrochim. Acta* **50** 4674-82

[4]   Sprague M J, Zheng J and Song C 2002 *Preprints - American Chemical Society, Division of Petroleum Chemistry* **47** 103-5

[5]   Pawelec B, La Parola V, Thomas S and Fierro J L G 2006 *J. Mol. Catal. A: Chemical* **253** 30-43

[6]   Magyar S, Hancsok J and Kallo D 2005 *Fuel Process. Technol.* **86** 1151-64

[7]   Qian E W, Otani K, Li L, Ishihara A and Kabe T 2004 *J. Catal.* **221** 294-301

[8]   Johnstone R A W, Liu J-Y, Lu L and Whittaker D 2003 *J. Mol. Catal. A: Chemical* **191** 289-94

[9]   Navarro R M, Pawelec B, Trejo J M, Mariscal R and Fierro J L G 2000 *J. Catal.* **189** 184-94

[10]   Murcia-Mascaros S, Pawelec B and Fierro J L G 2002 *Catal. Comm.* **3** 305-11

[11]   Thomas K, Binet C, Chevreau T, Cornet D and Gilson J P 2002 *J. Catal.* **212** 63-75

[12]   Morlang A, Neuhausen U, Klementiev K V, Schutze F W, Miehe G, Fuess H and Lox E S 2005 *Appl. Catal. B: Environ.* **60** 191-9

[13]   Berezin M Y, Wan K-T, Friedman R M, Orth R G, Raman S N, Ho S V and Ebner J R 2000 *J. Mol. Catal. A: Chemical* **158** 567-76

[14]   Koutsopoulos S, Johannessen T, Eriksen K M and Fehrmann R 2006 *J. Catal.* **238** 206-13

[15]   Touroude R, Girard P, Maire G, Kizling J, Boutonnet-Kizling M and Stenius P 1992 *Colloids Surf.* **67** 9-19

[16]   Solla-Gullon J, Montiel V, Aldaz A and Clavilier J 2003 *J. Electrochem. Soc.* **150** E104-9

[17]   Wu M-L, Chen D-H and Huang T-C 2001 *J. Colloid Interface Sci.* **243** 102-8

[18]   Veisz B, Toth L, Teschner D, Paal Z, Gyorffy N, Wild U and Schlogl R 2005 *J. Mol. Catal. A: Chemical* **238** 56-62

[19]   Adlim M, Abu Bakar M, Liew K Y and Ismail J 2004 *J. Mol. Catal. A: Chemical* **212** 141-9

[20]   Shevchenko E V, Talapin D V, Rogach A L, Kornowski A, Haase M and Weller

H 2002 *J. Am. Chem. Soc.* **124** 11480-5

[21]   Kim S W, Park J, Jang Y, Chung Y, Hwang S, Hyeon T and Kim Y W 2003 *Nano

Lett.* **3** 1289-91

[22]   Pawelec B, La Parola V, Navarro R M, Murcia-Mascaros S and Fierro J L G 2006

Carbon **44** 84-98

[23]   Lin X M, Sorensen C M and Klabunde K J 2000 *J. Nanopart. Res.* **2** 157-64

[24]   Samia A C S, Schlueter J A, Jiang J S, Bader S D, Qin C J and Lin X M 2006

Chem. Mater. **18** 5203-12

[25]   Samia A C S, Hyzer K, Schlueter J A, Qin C J, Jiang J S, Bader S D and Lin X M

2005 *J. Am. Chem. Soc.* **127** 4126-7

[26]   Shevchenko E V, Talapin D V, Schnablegger H, Kornowski A, Festin O,

Svedlindh P, Haase M and Weller H 2003 *J. Am. Chem. Soc.* **125** 9090-101
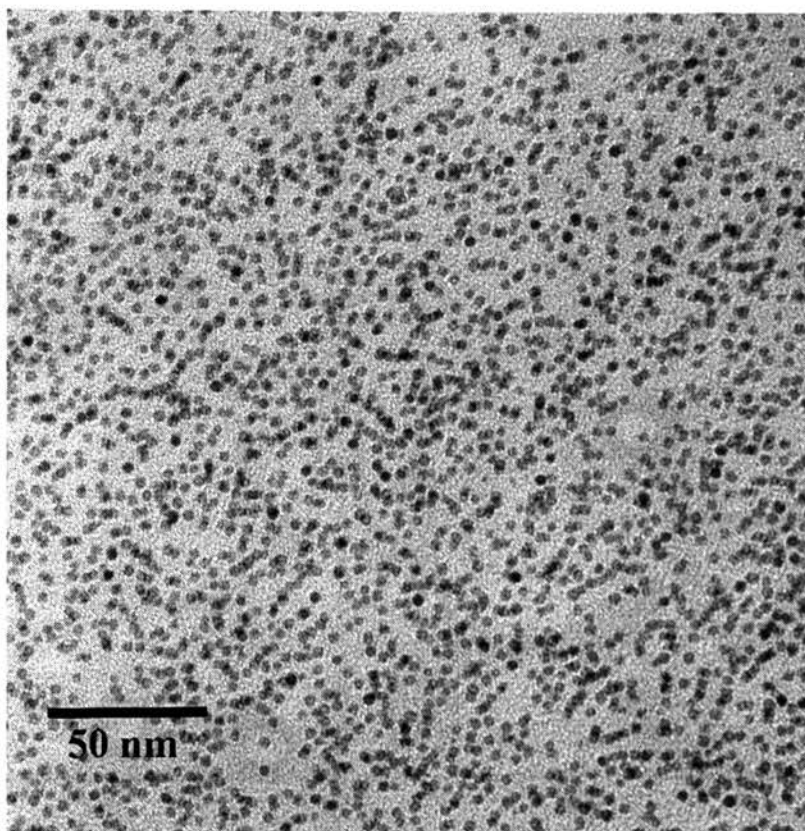
[27]   Ren G and Xing Y 2006 *Nanotech.* **17** 5596-601

Figure 1. A typical TEM image of the Pd-Pt alloy nanoparticles with an average size of 3.5 nm.
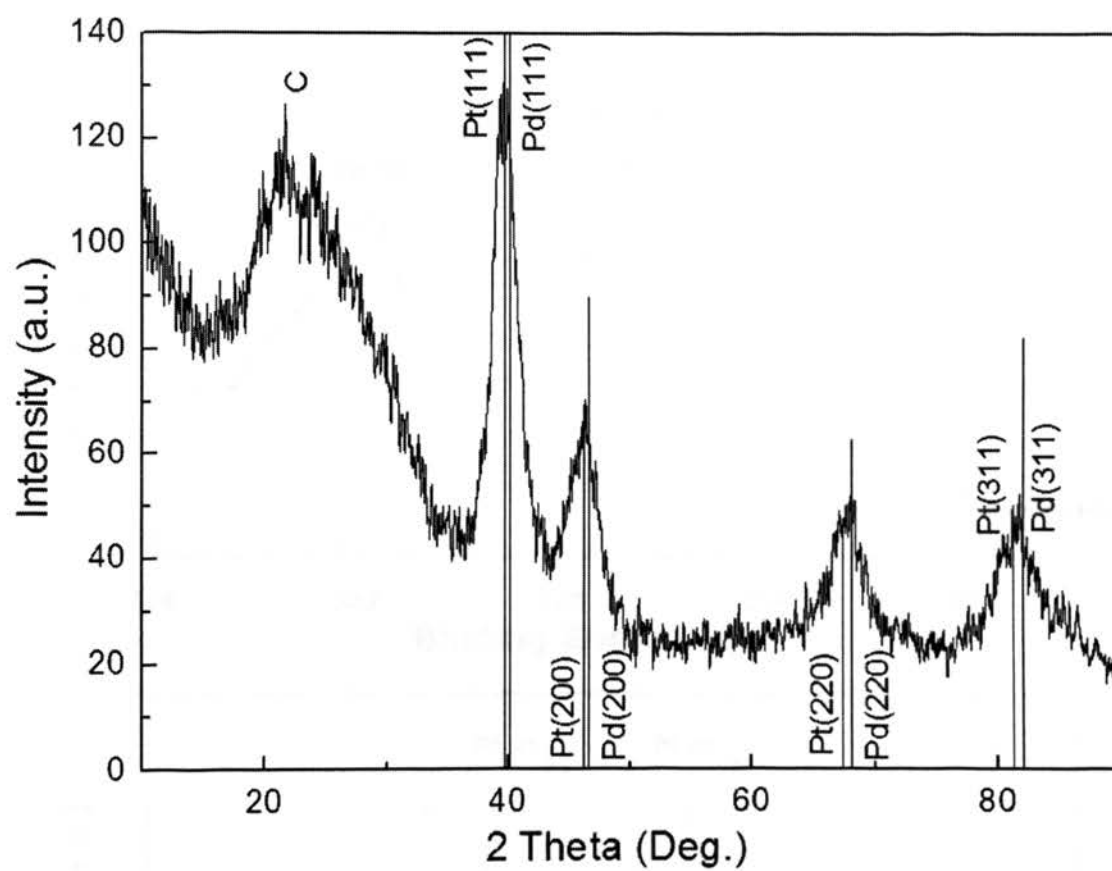
Figure 2. XRD pattern of the synthesized Pd-Pt nanoparticles supported on carbon.
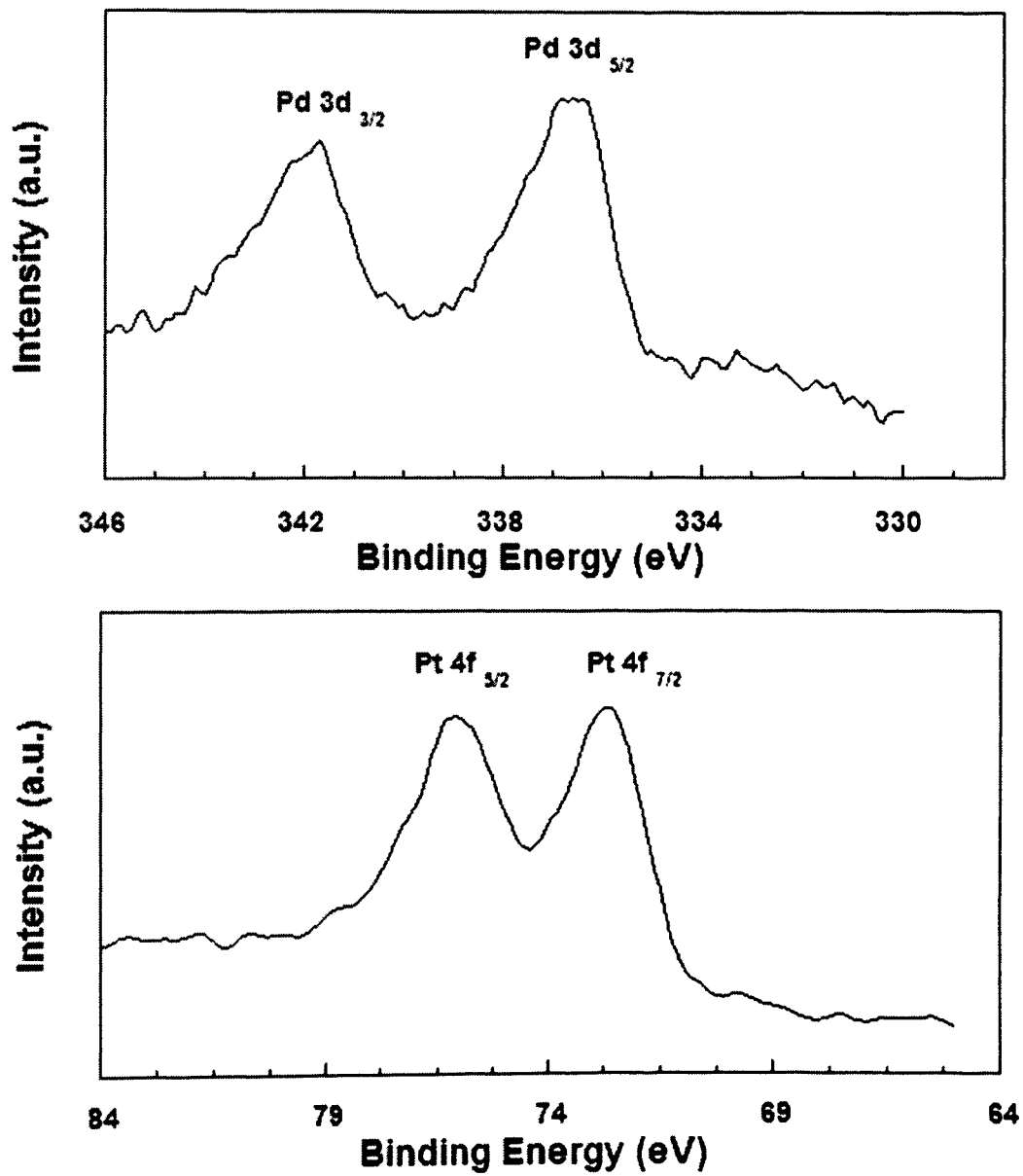
Figure 3. XPS window scans of the synthesized Pd-Pt nanoparticles supported on carbon.

Figure 4. Morphological evolution of the Pd-Pt nanoparticles during the synthesis: (a) – (f) show the nanoparticles collected at 3, 5, 10, 30, 40 and 120 min durations, respectively. The nanoparticle size remained unchanged after 10 min.
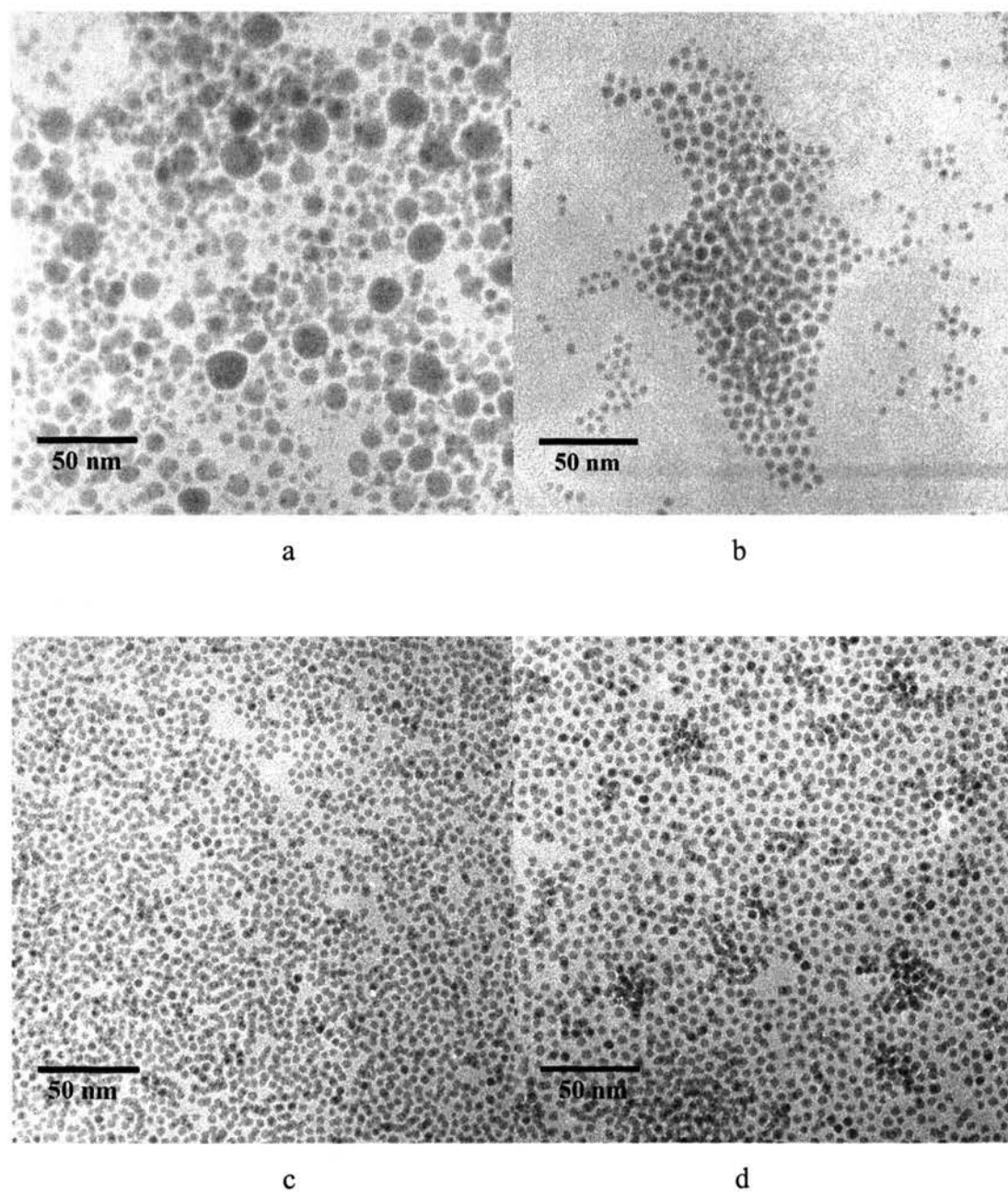
Figure 4. Morphological evolution of the Pd-Pt nanoparticles during the synthesis: (a) – (f) show the nanoparticles collected at 3, 5, 10, 30, 40 and 120 min durations, respectively. The nanoparticle size remained unchanged after 10 min. (cont.)
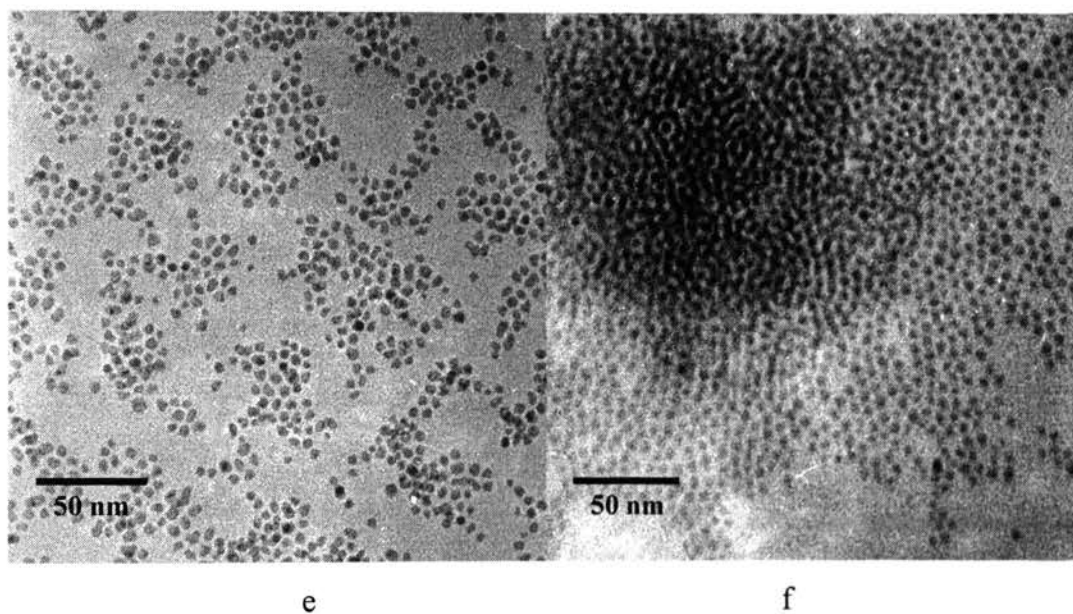
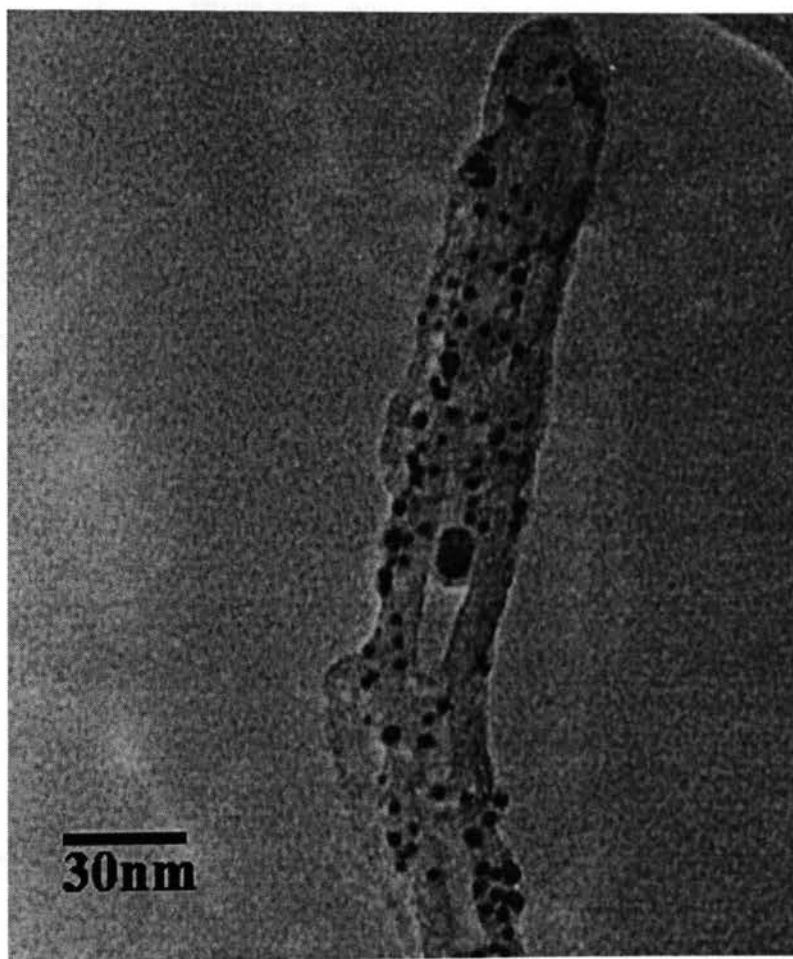**Figure 4.** TEM image of sintered PtPd nanoparticles on CNTs heat treated at 300 °C.
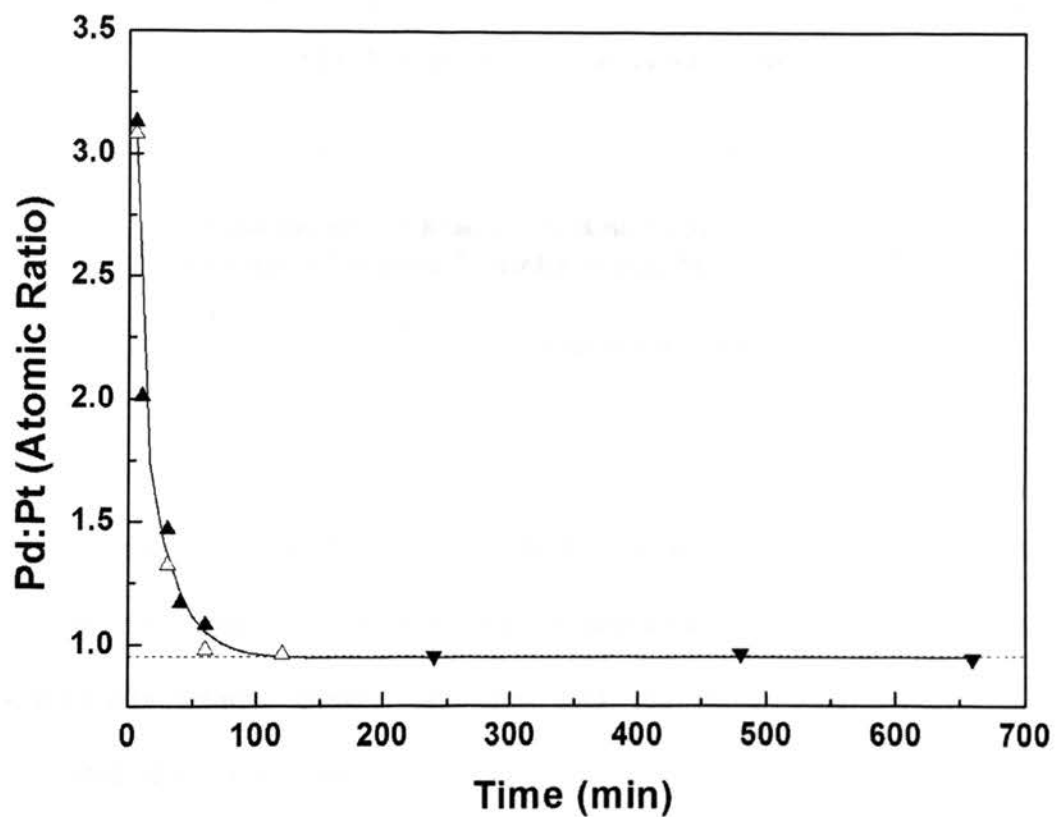
Figure 5. Alloy composition evolution of the Pd-Pt nanoparticles. The Pd to Pt atomic ratio reaches the preset ratio only after 120 min. Solid and open symbols represent results from three experiments. The solid line is a second order exponential fit line. The dotted line indicates the preset ratio of the alloy at Pd:Pt = 0.95.

PAPER II

DEPOSITION OF METALLIC NANOPARTICLES ON CARBON NANOTUBES VIA A FAST EVAPORATION PROCESS

Guoqiang Ren and Yangchuan Xing

Department of Chemical & Biological Engineering
University of Missouri – Rolla, Rolla, MO, U.S.A 65409

Email: xingy@umr.edu

Abstract

A new technique was developed for the deposition of colloidal metal nanoparticles on carbon nanotubes. It involves fast evaporation of a suspension containing sonochemically treated carbon nanotubes and the metal nanoparticles. It was demonstrated that metal nanoparticles with different sizes and concentrations can be deposited on the carbon nanotubes with few agglomerates. The technique seems to be not limited by what the nanoparticles are, and therefore would be applicable for other nanoparticles. The surfactants that were used to disperse the nanoparticles were found to hinder the nanoparticle deposition. When the nanoparticles were washed by ethanol, they can be well deposited on the carbon nanotubes. PtPd and $CoPt_3$ alloy nanoparticles were used to demonstrate the deposition processes. The obtained carbon nanotube supported nanoparticles were characterized by transmission electron microscopy, energy dispersive X-ray spectroscopy, X-ray photoelectron spectroscopy, and cyclic voltammetry.

1. Introduction

Carbon nanotubes (CNTs) functionalized with metallic nanoparticles [1] have been investigated extensively in recent years due to their added values and applications in, for example, heterogeneous catalysis [2-9], hydrogen storage [10], and sensors [11-13]. A variety of metallic nanoparticles have been successfully deposited onto CNTs, including Au [14-17], Ag [16, 18], Pt [4, 16, 19-21], Pd [11, 16, 18, 22], Ni [23-25], Pt-Ru [8, 18, 26-29], and FeNi [30]. Nanoparticle deposition techniques include chemical vapor deposition [11], surface modification and linking (reduction, impregnation) in aqueous solutions [14, 15, 19, 28, 31], solid state reactions [16], electrochemical deposition [20, 22, 24, 27], electroless deposition [25], γ-irradiation [18, 29], and wet chemistry [30]. These techniques, however, are often limited by the surface state of the CNTs and the deposited nanoparticles have problems of non-uniform surface deposition, broad nanoparticle sizes, and uncontrolled number density on the CNTs.

In this paper, we report a new technique to deposit metallic nanoparticles on CNTs. The new technique involves fast evaporating a hexane suspension of metallic nanoparticles and sonochemically functionalized CNTs. Upon fast drying, metallic nanoparticles were found to attach to the surface of CNTs fairly uniformly. Since the nanoparticles were synthesized in a separate colloidal process with surfactant protection, their size can be tightly controlled. By using different concentrations of the nanoparticle colloids, the particle number density on the CNTs can be controlled. The deposition process does not seem to be limited by what the nanoparticles are. As long as the nanoparticles can form a colloidal solution, they can be deposited onto the CNTs. Therefore, this technique appears to be universal. Here we demonstrate the successful

deposition of PtPd and CoPt$_3$ nanoparticles on multiwalled CNTs. These nanoparticles have different sizes and different concentrations of PtPd colloids were used. The electrochemical activities of these nanoparticles on CNTs were also demonstrated using cyclic voltammetry, considering these nanoparticles to be potential polymer electrolyte membrane fuel cell catalysts.

2. Experimental Details

The chemicals used in this work include platinum 2,4-pentanedionate (Pt(acac)$_2$), palladium 2,4-pentanedionate (Pd(acac)$_2$), trioctylphosphine (TOP), 1-adamantanecarboxylic acid (ACA), 1-hexadecylamine (HDA), dichlorobenzene (DCB), and diphenyl either (DPE), all purchased from Sigma Aldrich. Cobalt carbonyl was purchased from Alfa Aesar. Oleic acid (OA) and oleyamine were from Sigma Aldrich. Multiwalled carbon nanotubes (CNTs) were from NanoLab, Inc. and functionalized in our laboratory using a sonochemical technique developed previously [21, 32].

PtPd nanoparticles were synthesized using a hot organometallic process, in which the precursor Pt(acac)$_2$ was reduced by 1,2-diol [33] and Pd(acac)$_2$-TOP complex was thermally decomposed [34] in the presence of ACA and HDA as surfactants. The details of the synthesis procedure will be reported in a separate paper. In this work we only used the PtPd nanoparticles that were dispersed in hexane. The average particle PtPd size used in this work is 3.5 nm. The synthesis of CoPt$_3$ was obtained following a previously reported technique [35]. This technique involves thermal decomposition of cobalt carbonyl and simultaneously reduction of Pt(acac)$_2$ in dichlorobenzene with OA as the

surfactant and oleyamine as co-surfactant. The $CoPt_3$ nanoparticles used in this work were also dispersed in hexane and have an average particle size of 10.5 nm.

Deposition of the metallic nanoparticles on the CNTs was achieved by a fast evaporation technique developed in our laboratory. In this technique, 6.0 mg sonochemically-treated dry CNT powders were added into a glass vial containing 10.0 mL hexane and dispersed fully in an ultrasonic bath (Fischer Scientific, Model 30H) for 2 h at 60°C. A certain volume of the nanoparticle colloid solution of hexane was added to the vial depending on the desired nanoparticle loading. The vial was ultrasonically mixed for another 5 min to form a suspension of the nanoparticles and CNTs. This suspension was heated and concentrated to 4.0 mL on a stirrer/heater. The vial was again put back in the ultrasonic bath at 60°C, uncovered, until the solvent was fully evaporated. The suspension evaporated rapidly and became dry in about 30 min. A black material containing the CNTs and the nanoparticles was then obtained. The material was scratched off the wall of the vial, heat treated at 200 °C in 10% H_2 in N_2, and analyzed for their properties.

Characterization of the nanoparticles on CNTs was achieved using a transmission electron microscope (TEM, Philips EM 430) operating at 300kV. The TEM grid was prepared by dispersing a small amount of the material in hexane with ultrasonication. A drop of the dispersion was transferred with a pipette and put on a TEM grid (400-mesh carbon-coated copper grid, Electron Microscopy Sciences). The drop on the grid was allowed to dry under open atmosphere. The grid was then examined with the TEM, and images were taken. Image analysis includes measurement of the diameters of ~500 nanoparticles and a statistical result of the size was obtained by regression. Energy

dispersive X-ray spectroscopy (EDS, Noran Voyager III light element EDS system) analysis of the specimen was performed. To enhance the signal to noise ratio, the TEM sample holder was tilted 20° towards the EDS detector.

X-ray photoelectron spectroscopy (XPS) measurements were performed on a Kratos Axis 165 XPS spectrometer. The spectrometer is equipped with a concentric hemispherical analyzer (CHA) which uses 8 channeltron detectors. The sample was ion sputtered with a differential ion gun for 60 seconds at 4 kV. A Mg Kα anode, operated at 15kV and 225 W with a photon energy of $hv = 1253.6$ eV, was used as the X-ray source. The base pressure of the chamber during inspection was 10^{-9} Torr. The pass energy was 80 eV during the survey scan and 20 eV for the windows scan.

Electrochemical activity measurements were conducted using cyclic voltammetry (CV) in a 1.0 M H_2SO_4 solution. The experiments were performed at room temperature using an Electrochemical Workstation (BAS100, Bioanalytical Sciences). The working electrode was prepared as follows [36]. A glassy carbon disk (3 mm in diameter) was polished to a mirror finish using alumina pastes. A small drop of ethanol solution dispersed with the CNT supported nanoparticles was put on the glassy carbon with a pipette. After drying, a drop of Nafion solution (5 wt. % in water) was put on the electrode as a binder and electrolyte. The electrode was dried at 70 °C and ready for measurements. The thin film electrode was then put in an electrochemical cell (C3 Cell, Bioanalytical Sciences). Potential scans were at 50 mV/s with a Ag/AgCl reference electrode and a platinum wire coil counter electrode.

3. Results and Discussion

Figure 1 shows a typical TEM image of the PtPd nanoparticles before they were deposited on the CNTs. Also shown are the EDS spectrum and the size distribution histogram. It can be seen that the PtPd nanoparticles are monodisperse and uniform with a spherical shape. The statistical size distribution of the PtPd nanoparticles was obtained by measuring the nanoparticles from the obtained TEM images. The mean size was calculated to be 3.5 ± 0.3 nm in diameter. The EDS spectrum indicated a bimetallic composition of Pt and Pd. The small amount of silicon was from the EDS detector, which is made of lithium-drifted silicon (Si(Li)). Carbon and copper were from the carbon-coated copper TEM grids. Figure 2 shows a similar result for the $CoPt_3$ nanoparticles before they were deposited on the CNTs. The $CoPt_3$ nanoparticles are much larger than the PtPd nanoparticles with an average size of 10.5 ± 1.6 nm in diameter and have irregular shapes. The EDS spectrum confirmed the existence of Pt and Co.

Figure 3 shows the PtPd nanoparticles deposited on the CNTs, with two different concentrations of PtPd nanoparticles. It can be seen that the PtPd nanoparticles are located on the outer surface of CNTs and both the size and uniformity of the nanoparticles remains unchanged with the deposition technique. To ensure strong attachment of the nanoparticles on the CNTs, they had been treated at 200 °C in a hydrogen-nitrogen gas after the nanoparticle deposition was done. The heat treatment was also to remove any residue organics on the nanoparticles so that the electrochemical activity can be studied. However, heat treatment temperatures above 200 °C were found to result in sintering of the PtPd nanoparticles (Figure 4). The TEM images in Figure 3

clearly showed that at the lower nanoparticle concentration the PtPd nanoparticles were distributed better on the CNTs. At the higher nanoparticle concentration, the surface of CNTs was nearly 80% covered with the PtPd nanoparticles and in some regions, agglomerates of the nanoparticles were formed. Wherever aggregations of the nanotubes were found, the supported nanoparticles became hardly distinguished due to overlapping. Figure 5 shows CoPt$_3$ nanoparticles deposited on the CNTs. The CoPt$_3$ nanoparticles are relatively evenly distributed on the CNTs, though a few agglomerates were also observed. Both the PtPd and CoPt$_3$ nanoparticles were seen to have direct contact with the CNT surface before and after the heat treatment.

During the nanoparticle deposition process, both the nanoparticles and the CNTs were assumed to be well dispersed and finely mixed in the solvent (hexane) by sonication. The main idea in the evaporation process was to have fast evaporation of solvent to reduce nanoparticle agglomeration. In theory, any solvent can be used, but a low boiling point solvent would allow operation at a lower temperature. Hexane was used in this work which has a boiling point of 69 $^{\circ}$C in open atmosphere. At a bath temperature of 60 $^{\circ}$C, sprinkling was observed at the surface of the suspension. This was believed to be the result of ultrasonic agitation. With the evaporation of the solvent, the nanoparticles were believed to be physically deposited onto the surface of CNTs. Although the nanoparticles were synthesized with surfactant protection, they were washed several times with ethanol before being used for their deposition. We found that if they were not washed, the nanoparticles could not be deposited uniformly on the CNTs and the particle number density was much lower than deposited with the washed nanoparticles. We believe that the surface functional groups had an adverse effect for the

nanoparticle deposition during the evaporation process. Without surfactants for nanoparticle dispersion, however, the nanoparticles have to be dispersed with ultrasonic agitation.

When the hexane was evaporated to the last amount that can only wet the CNTs, they must have formed a liquid film (or coating) on the CNTs with the nanoparticles dispersed inside, so that further drying would leave the nanoparticles distributed uniformly on the CNTs. If the solvent did not wet the CNTs and formed separate liquid drops, then the nanoparticles would have eventually formed agglomerates when the solvent was completely evaporated, as schematically illustrated in Figure 6. We have shown previously that the sonochemically treated CNTs have a majority of carbonyl groups on their surfaces. These groups were attributed to partial wetting of the CNTs by hexane, which was evidenced by that the CNT powders, once ultrasonically dispersed in hexane, can form a stable colloid for a short time.

XPS was used to study the oxidation state of the nanoparticles on the CNTs. The XPS results for PtPd/CNT and CoPt$_3$/CNT (Figure 7) confirmed the existence of Pt and Pd, and Co and Pt on the surface of CNTs, respectively. The XPS results showed that there were negligible metal oxides in the samples, confirming that the nanoparticles are in a metallic state. However, the atomic ratio between Pt and Pd, based on Pt$_{4f}$ and Pd$_{3d}$ peaks, was calculated to be 1:1.2; the ratio between Co and Pt for CoPt$_3$, based on Co$_{2p}$ and Pt$_{4f}$ peaks, was approximately 1.87:1. Comparing these atomic ratios with the values known of the original compositions, we concluded that there is a surface deficiency in both cases for the Pt. One explanation for this Pt deficiency could be that the nanoparticles during the high temperature synthesis would tend to lower their surface

energy. To have the Pt on the surface, the surface energies would be higher since Pt has higher surface energy than that of either Pd or Co. Another explanation could be that the sputtering before XPS measurement may have changed the surface compositions. Strong bombardment of ions may cause ion-assisted mass transport of surface atoms, resulting in redistribution over the whole particles. Further evidence is needed to elucidate the surface segregation effects [37, 38].

As potential electrocatalysts for polymer electrolyte fuel cells, the CNT supported metal nanoparticles were preliminarily studied using cyclic voltammetry. Figure 8 shows the voltammograms for the PtPt and $CoPt_3$ nanoparticles on CNTs. Both nanoparticles on CNTs showed electrochemical activities in the adsorption/desorption regions. However, it can be seen that the characteristic peaks for the Pt in the hydrogen adsorption/desorption region are no longer apparent [39]. The characteristic adsorption peak at ~0.12 V for the Pt(110) habits and that at ~ 0.25 V for Pt(100) habits did not show up. This was attributed to the alloying effects of the metallic nanoparticles.

4. Conclusions

A fast evaporation technique was developed to deposit metallic nanoparticles on multiwalled CNTs. With this technique, we have demonstrated the deposition of PtPd and $CoPt_3$ nanoparticles. These nanoparticles can be deposited on the CNTs with uniform distributions. It was found that the surfactants that were used to cap the nanoparticles hindered the nanoparticle deposition on the nanotubes. With washed nanoparticles, good deposition results were obtained. Since this evaporation deposition process involves physical process only, it was concluded that the application of this

method is not limited to the nanoparticles demonstrated in this work; other nanoparticles should also be deposited with this technique. The process does not seem to be limited by its scale, and large-scale deposition of nanoparticles onto CNTs would be possible. In addition, this process has the advantages of that the nanoparticle size and number density on the CNTs can be independently controlled, opening ways of obtaining tailored nanomaterials.

5. Acknowledgement

References

[1]   Satishkumar B C, Vogl E M, Govindaraj A and Rao C N R 1996 *J. Phy. D: Appl. Phys.* **29** 3173-6

[2]   Planeix J M, Coustel N, Coq B, Brotons V, Kumbhar P S, Dutartre R, Geneste P, Bernier P and Ajayan P M 1994 *J. Am. Chem. Soc.* **116** 7935-6

[3]   Pawelec B, La Parola V, Navarro R M, Murcia-Mascaros S and Fierro J L G 2006 *Carbon* **44** 84-98

[4]   Kim Y-T and Mitani T 2006 *J. Catal.* **238** 394-401

[5]   Liu Z, Lin X, Lee J Y, Zhang W, Han M and Gan L M 2002 *Langmuir* **18** 4054-60

[6] Mu Y, Liang H, Hu J, Jiang L and Wan L 2005 *J. Phys. Chem. B* **109** 22212-6

[7] Wang H J, Yu H, Peng F and Lv P 2006 *Electrochem. Comm.* **8** 499-504

[8] Yao Y-l, Ding Y, Ye L-S and Xia X-H 2006 *Carbon* **44** 61-6

[9] Zhao X, Li W, Jiang L, Zhou W, Xin Q, Yi B and Sun G 2004 *Carbon* **42** 3263-5

[10] Mu S-c, Tang H-l, Qian S-h, Pan M and Yuan R-z 2006 *Carbon* **44** 762-7

[11] Kong J, Chapline M G and Dai H 2001 *Adv. Mater.* **13** 1384-6

[12] Yang M, Jiang J, Yang Y, Chen X, Shen G and Yu R 2006 *Biosens. and Bioelectron.* **21** 1791-7

[13] Song Z, Huang J-D, Wu B-Y, Shi H-B, Anzai J-I and Chen Q 2006 *Sensors and Actuators B: Chemical* **115** 626-33

[14] Ou Y Y and Huang M H 2006 *J. Phys. Chem. B* **110** 2031-6

[15] Jiang K, Eitan A, Schadler L S, Ajayan P M, Siegel R W, Grobert N, Mayne M, Reyes-Reyes M, Terrones H and Terrones M 2003 *Nano Lett.* **3** 275-7

[16] Xue B, Chen P, Hong Q, Lin J and Tan K L 2001 *J. Mater. Chem.* **11** 2378-81

[17] Jiang L and Gao L 2003 *Carbon* **41** 2923-9

[18] Oh S-D, So B-K, Choi S-H, Gopalan A, Lee K-P, Ro Yoon K and Choi I S 2005 *Mater. Lett.* **59** 1121-4

[19] Xie J, Zhang N and Varadan V K 2006 *Smart Mater. Struct.* **15** S5-8

[20] Waje M M, Wang X, Li W and Yan Y 2005 *Nanotechnology* **16** S395-400

[21] Xing Y 2004 *J. Phys. Chem. B* **108** 19255-9

[22] Guo D-J and Li H-L 2005 *J. Colloid Interface Sci.* **286** 274-9

[23] Cheng J, Zhang X and Ye Y 2006 *J. Solid State Chem.* **179** 91-5

[24] Xu Q, Zhang L and Zhu J 2003 *J. Phys. Chem. B* **107** 8294-6

[25] Wang F, Arai S, Park K C, Takeuchi K, Kim Y J and Endo M 2006 *Carbon* **44** 1307-10

[26] Rajesh B, Thampi K R, Bonard J-M and Viswanathan B 2000 *J. Mater. Chem.* **10** 1757-9

[27] He Z, Chen J, Liu D, Zhou H and Kuang Y 2004 *Diamond Related Mater.* **13** 1764-70

[28] Chien C-C and Jeng K-T 2006 *Mater. Chem. Phys.* **99** 80-7

[29] Oh S-D, Yoon K R, Choi S-H, Gopalan A, Lee K-P, Sohn S-H, Kang H-D and Choi I S 2006 *J. Non-Crystalline Solids* **352** 355-60

[30] Wu H-Q, Cao Y-J, Yuan P-S, Xu H-Y and Wei X-W 2005 *Chem. Phys. Lett.* **406** 148-53

[31] Yu Y, Ma L-L, Huang W-Y, Li J-L, Wong P-K and Yu J C 2005 *J. Solid State Chem.* **178** 1488-94

[32] Xing Y, Li L, Chusuei C C and Hull R V 2005 *Langmuir* **21** 4185-90

[33] Shevchenko E V, Talapin D V, Rogach A L, Kornowski A, Haase M and Weller H 2002 *J. Am. Chem. Soc.* **124** 11480-5

[34] Kim S W, Park J, Jang Y, Chung Y, Hwang S, Hyeon T and Kim Y W 2003 *Nano Lett.* **3** 1289-91

[35] Shevchenko E V, Talapin D V, Schnablegger H, Kornowski A, Festin O, Svedlindh P, Haase M and Weller H 2003 *J. Am. Chem. Soc.* **125** 9090-101

[36] Schmidt T J, Gasteiger H A, Stab G D, Urban P M, Kolb D M and Behm R J 1998 *J. Electrochem. Soc.* **145** 2354-8

[37] Ramirez Caballero G E and Balbuena P B 2006 *Mol. Simulation* **32** 297-303

[38] Chui Y H and Chan K-Y 2005 *Chem. Phys. Lett.* **408** 49-53
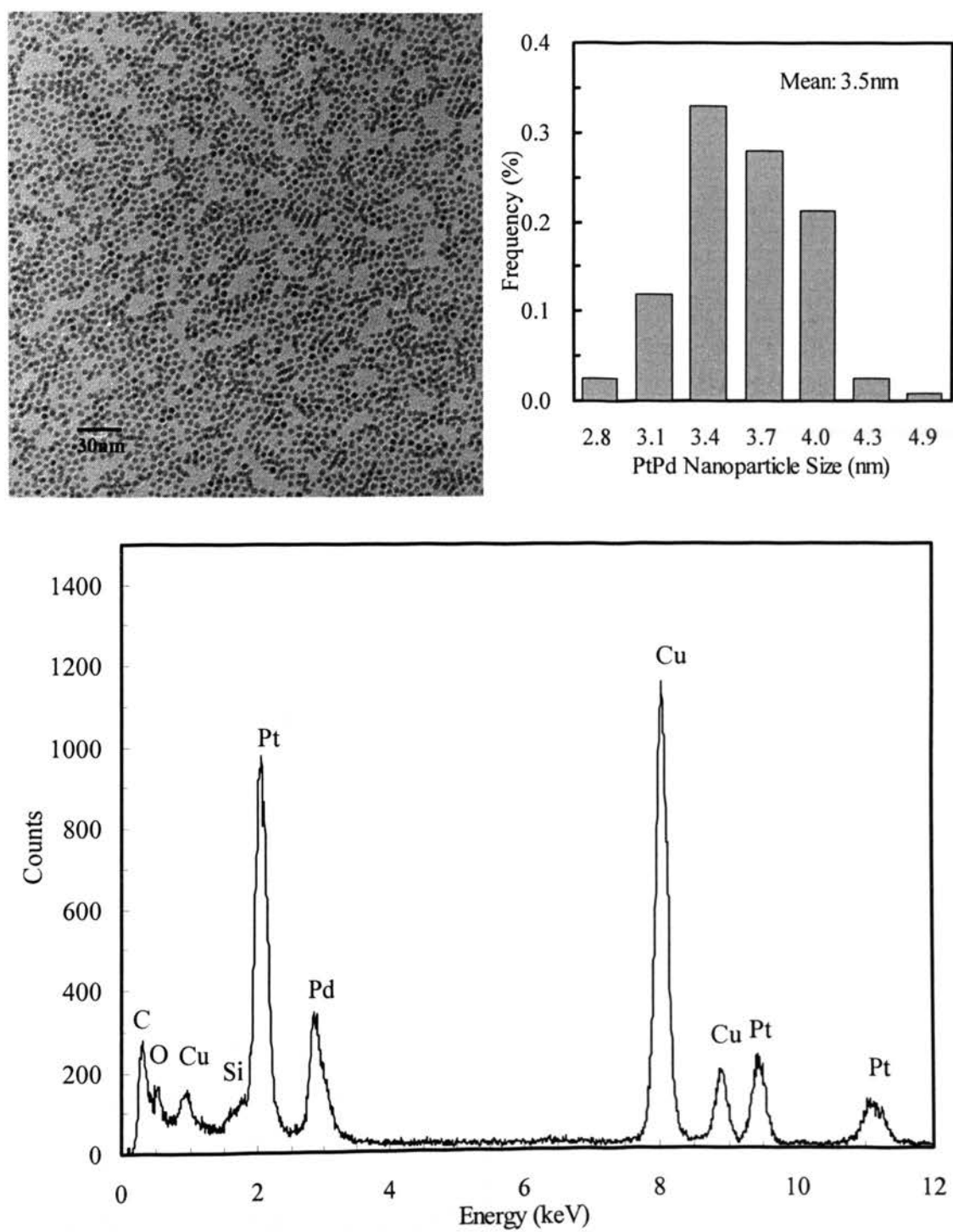
[39] Woods R 1976 *Electroanal. Chem.* **9** 1

Figure 1. (a) TEM image of PtPd nanoparticles, (b) size distribution histogram, and (c) EDS spectrum of PtPd nanoparticles.
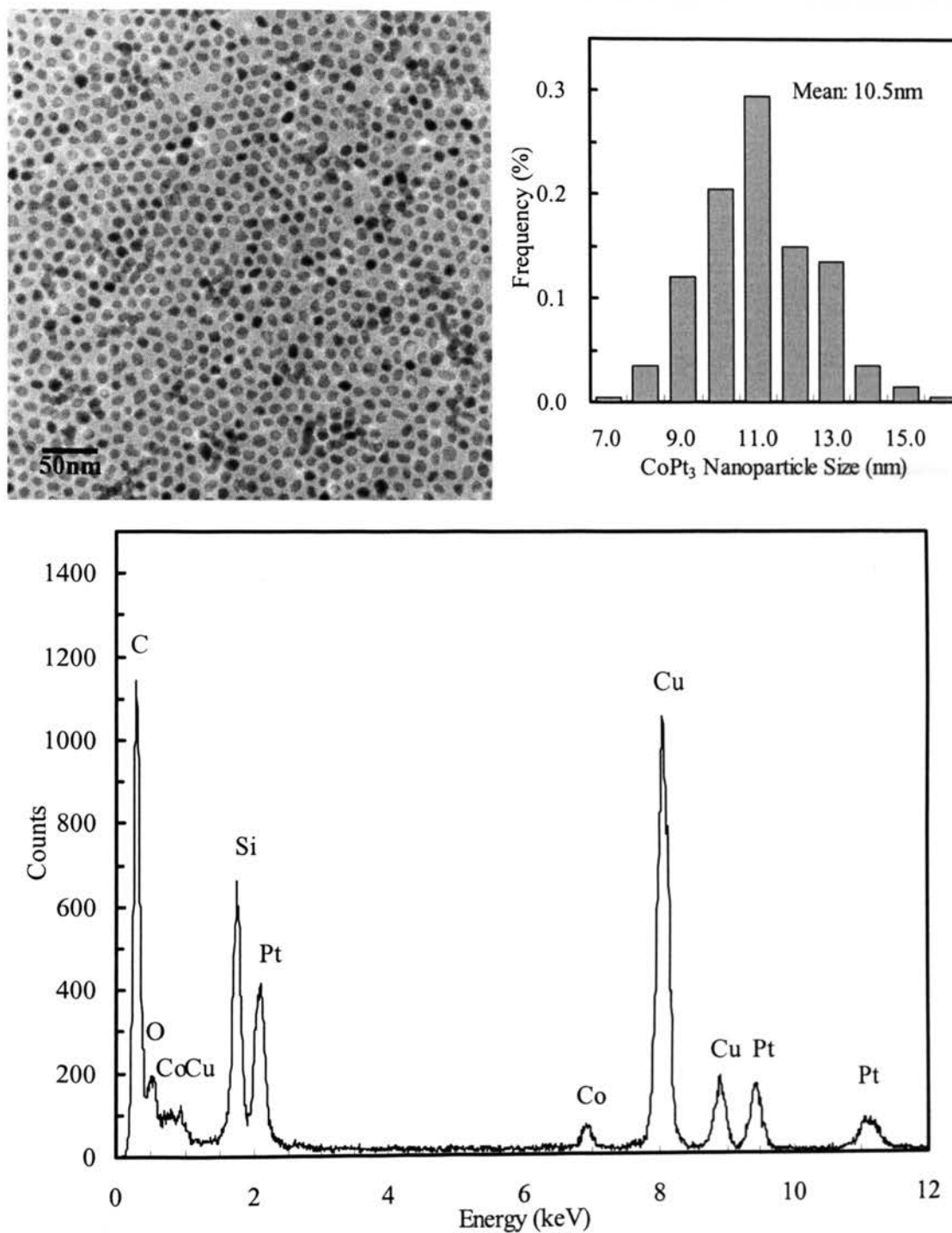
Figure 2. (a) TEM image of CoPt$_3$ nanoparticles, (b) size distribution histogram, and (c) EDS spectrum of PtPd nanoparticles.
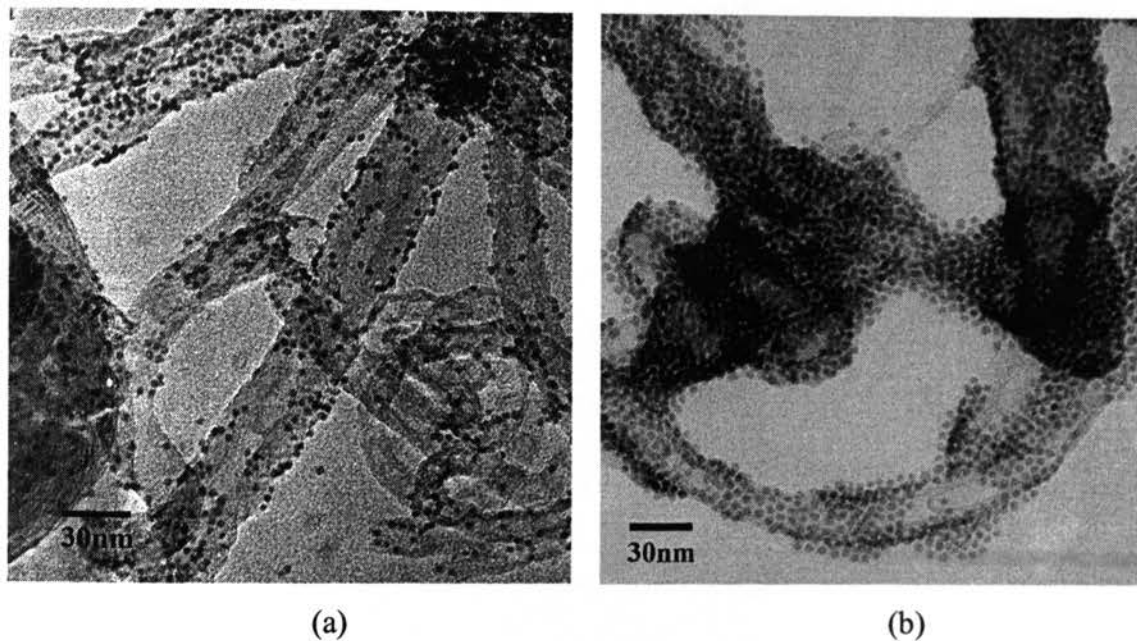
(a)   (b)

Figure 3. TEM images of the PtPd nanoparticles deposited on CNTs at two nanoparticle concentrations.
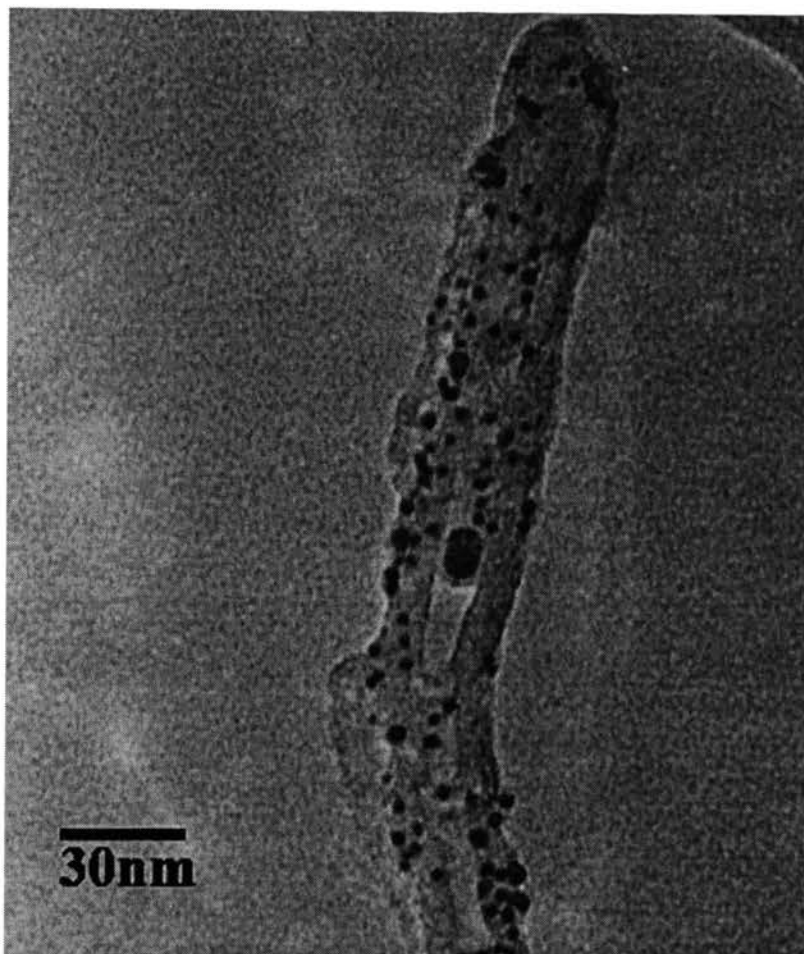
Figure 4. TEM image of sintered PtPd nanoparticles on CNTs heat treated at 300 °C.
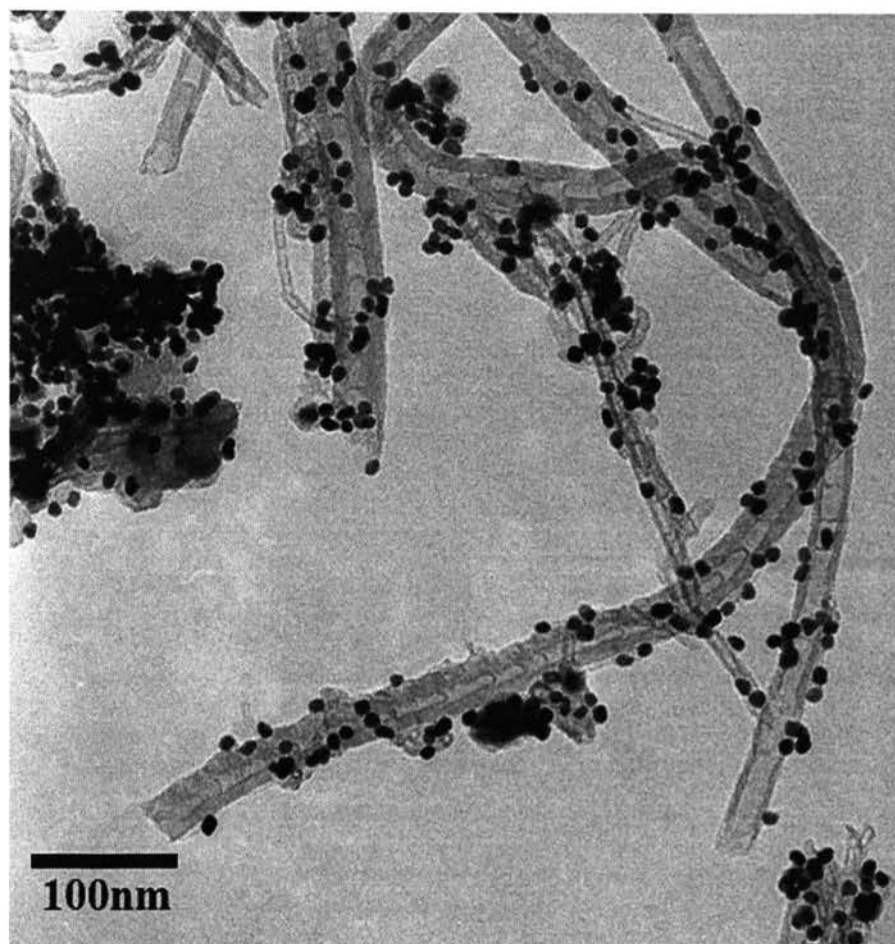
Figure 5. TEM image of the CoPt$_3$ nanoparticles deposited on CNTs.
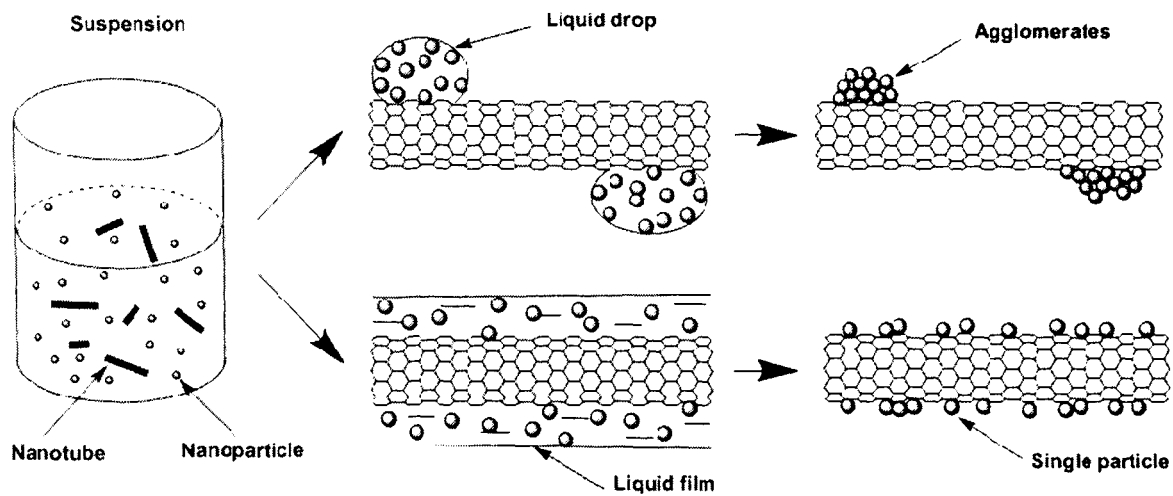
Figure 6. An illustration of evaporation deposition process of nanoparticles on CNTs forming agglomerate or individual nanoparticles.
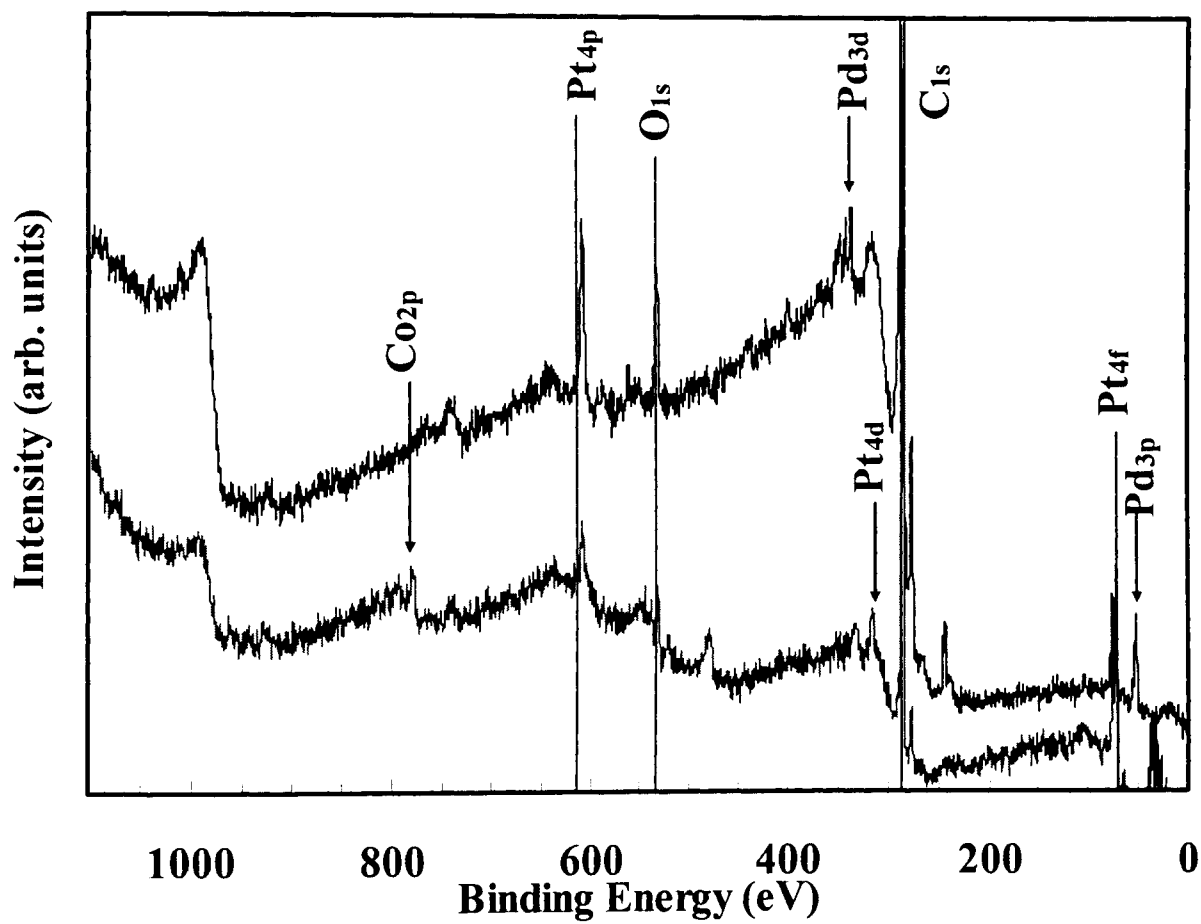
Figure 7. XPS spectra of the PtPd/CNT and CoPt₃/CNT, showing the metallic elements.
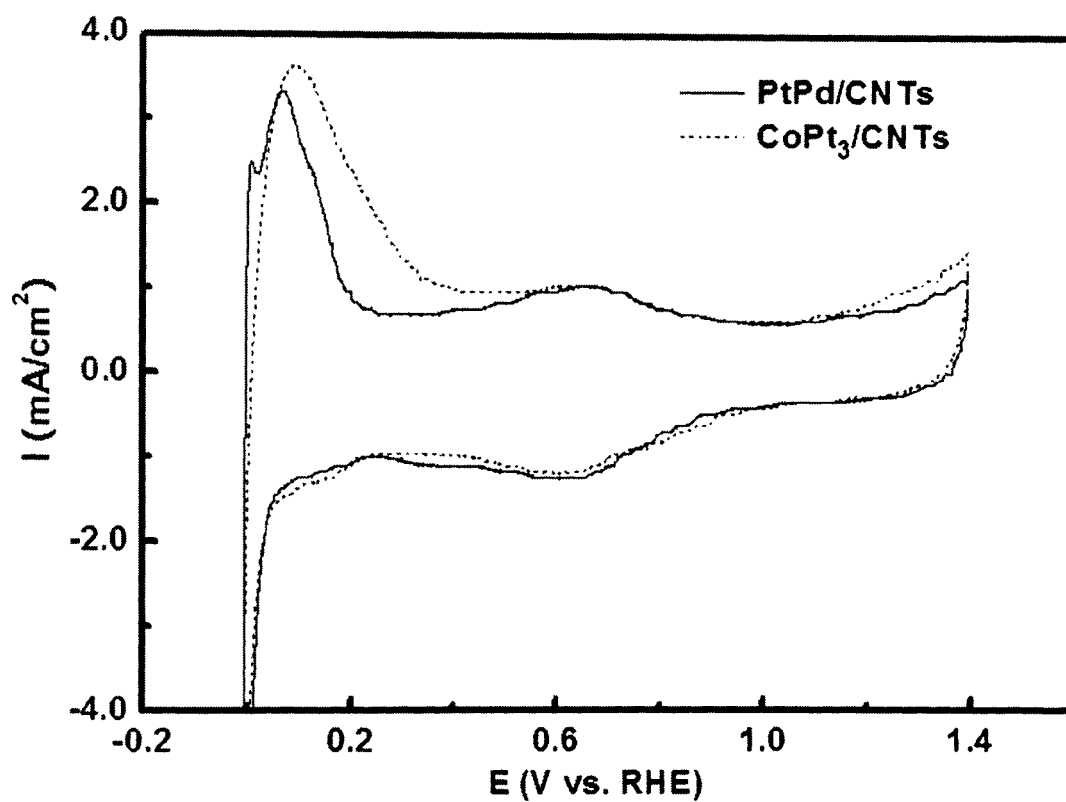
Figure 8. Cyclic voltammograms of the PtPd/CNT and CoPt₃/CNT conducted in 1.0 M H₂SO₄ electrolyte with scan rate of 50 mV/s.

APPENDIX

Temperature-Induced Restructuring of Pd-Pt Superlattices

Introduction

Engineering of nanoscale materials at the macroscopic level has received considerable attention due to the difficulty or inability to manipulate the single microscopic nanoparticles. Self-assembly of nanoparticles into 1D, 2D and 3D superlattices with various patterns is considered the most effective way to control the macroscopic morphology and properties of disordered nanoparticle dispersions. Nanoparticles, usually with sizes ranging from several to tens of nanometers, are vulnerable to environment fluctuations such as temperature (heat), vibrations and gravity during their self-assembling process.

In this work, we prepared PtPd superlattices at room temperatures and investigated the temperature effect on the restructuring of the PtPd superlattices at elevated temperatures. The PtPd nanoparticles we used were spherical nanoparticles at around 3.5 nm and had a narrow size distribution ($\pm$ 0.3 nm). The surfactants used to assist dispersion consisted of oleic acids and oleylamine (1:1, vol.). It was found that the critical temperature that induced the phase transition of PtPd superlattices from an ordered state to a disordered state fell into a range of 100 – 110 °C. Meanwhile, proper selection of a heat treatment temperature could restructure the less-ordered superlattices into better-ordered ones.

Experimental Methods

Preparation of PtPd Nanoparticle Superlattices

Synthesis of 3.5 nm PtPd bimetallic nanoparticles was accomplished by a hot organometallic route as reported in Paper I. The as-prepared PtPd nanoparticles were washed extensively with ethanol for 5 times to ensure that the organic coating was removed to the greatest extent. Half of the washed nanoparticles were used and redispersed in ~11.5 mL hexane and a drop of oleic acid (approx. 10.5 uL) and a drop of oleylamine (approx. 11.1 uL) were added to the 11.5 mL hexane dispersed PtPd colloidal nanoparticle suspension. This suspension was agitated in an ultrasonic bath for 5 min and allowed to stand for 5 min. A drop of the suspension was placed on a carbon-coated TEM copper grid on a glass slide at room temperature (23 °C), and the same procedure was repeated for each sample.

Temperature-Induced Structure Change of PtPd Superlattice

The as-prepared PtPd-deposited TEM grids were treated at different temperatures in a furnace (Lindberg/Blue) under the protection of hydrogen and nitrogen gases with a flow rate ratio of 1:10. To ensure the same procedures for all samples, after the samples were loaded into the chamber, they were heated to the preset temperature with the same time interval (10 min) and remained at that temperature for 30 min. The chamber was then exposed to open atmosphere and allowed to rapid cooling. The samples inside the chamber were under H_2/N_2 atmosphere. The preset temperatures for the heat treatment were 60 – 130 °C, with an increment of 10 °C and 50 – 250 °C with an increment of 100 °C. After heat treatment, the grids were investigated using TEM and an image that best

represented the samples was taken. These images were analyzed with respect to the superlattice structure, and when necessary, Fast Fourier Transform (FFT) of the images was performed.

Results and Discussions

The TEM images of the as-synthesized PtPd nanoparticles and their size distribution can be found in Paper II (Figure 1). The 3.5 ± 0.3 nm PtPd nanoparticles are quite uniform and as can be seen from the TEM images, the particles are mostly spherical. In this way, the size and shape effects of particles during self-assembly can be excluded. Figure A1 shows the as-obtained PtPd superlattices at room temperature (23 °C). Both 2D and 3D superlattices are identified in the images. The self-assembly of nanoparticles assisted with surfactants is a process that monolayer protected nanoparticles organize themselves under the regulation of van der Waals interactions among alkyl chains. This is a complex process and is sensitive to changes in the environment; in this work, we tried to keep the conditions unchanged for the same batch of 23°C self-assembled samples. However, different self-assembled structures could be found, of which the most obvious differences were between 2D and 3D superlattices. It was proposed that the 3D superlattices were formed directly in the colloidal suspension and precipitated to the grids upon evaporation of solvents. [1] Since we could not control the superlattice formation precisely, in the analysis, the structures that best represented the changes were chosen.

The TEM images of the heat-treated PtPd superlattices are given in Figure A2. Two images were taken, with a low magnification image shown on the left (1) and a high

magnification image on the right (2). The high magnification image represented part of the left image. In order to clarify the changes, the following definitions are given:

Long range order – If ordered structures or spot patterns can be identified in the low magnification images, we say that the sample bears a long range order;

Short range order – If ordered structures or spot patterns can be identified in the high magnification images, we say that the sample bears a short range order;

If a sample has long or short range order, we say that the sample is in an ordered state. Otherwise, we say that the sample is in a disordered state.

In Figure A2 (a-1), after heat treatment, ordered structures can still be found in the image, with both 2D and 3D superlattices. In the corresponding high magnification image, monolayers and bilayers of nanoparticles forming ordered superlattices are identified. As defined previously, we say that the 60 °C heat treated sample bears both long and short range orders. This statement also holds true for the 70 °C and 80 °C samples. In the 90 °C sample (d-1, d-2) and 100 °C sample (e-1, e-2), long range orders are found while no obvious short range orders are identified. In Figure A2 (f-h), both images represent a disordered state of the nanoparticle assembly. These samples are in a disordered state.

The changes from an ordered state to a disordered state take place somewhere between 100 and 110 °C. This transition is clearly shown in Figure A3. The same transition temperature range was reported by Chaki et al [2]. In their work, the transition temperature for dodecanethiol passivated Au nanoclusters superlattice was investigated by in situ low-angle XRD, and an irreversible phase transition from an ordered state to a

disordered state took place in a temperature range of 100-115 °C. Their result was also confirmed by in situ IR analysis. A simple comparison of their system with the PtPd superlattice can not clarify the consistence of the two phase transition range. The factors that can affect the restructuring may include nanoparticle size and shape, types of capping materials, nanoparticle-capping material interaction, nanoparticle-substrate interactions and heat treatment. More work needs to be done with regard to this aspect.

Another phenomenon that needs to be addressed is that after proper heat treatment, the lattice structures of the self-assembly tend to be better-ordered; and as the temperature increased, phase transition from 3D to 2D superlattice occurred, just like melting. Figure A4 gives the TEM images of the 50 - 250 °C (increment of 100 °C) heat treated PtPd superlattices, with both low magnification (left) and high magnification images (right). Images a-1 & a-2 represent the 23 °C sample, which can be considered as the original state of the superlattice before heat treatment. It is noticed that pieces of 2D and 3D superlattices, just like grains with sizes from 150 – 200 nm, exist in the low magnification image. The lattices are not very clear and the grain boundaries are blurry. A closer investigation of the lattices and grain boundaries at higher magnification (a-2) reveals that the nanoparticles self-assembled into distorted hexagons and the grain boundaries are hard to distinguish. After heat treatment at 50 °C, the sizes of the grains seem to grow, from 200 to 400 nm, compared with the 23 °C sample. Meanwhile, the lattice structures are better-ordered and clearer grain boundaries can be seen. As the temperature was raised to 150 °C, the superlattices melted and the hexagon structures were destroyed. Sintering of PtPd occurred at 250 °C, which corresponded well with the

previously observed sintering temperature at above 200 °C for PtPd nanoparticles supported on carbon nanotubes.

The structures of the restructured superlattices are investigated with Fast Fourier Transform (FFT). Part of images b-2 in Figure A4 is processed with ImageJ software and an FFT image is obtained, which is shown in Figure A5. In the FFT image, the vertical and horizontal lines may arise from the edge effect of the corresponding image and the clouds near the center may come from the low frequency information in the original image. Measurement of the spot spacings in the FFT image is achieved using imageJ software and the ratio of average spot spacings is 1.07:1:1.05 (starting from the vertical direction, and going counterclockwise). Although the hexagon structures are still distorted, it can be concluded that after heat treatment at 50 °C, the hexagon structures in the superlattices become better-ordered than the sample treated at 23 °C. Therefore, if proper heat treatment temperature is selected, temperature-induced superlattice restructuring may help produce better-ordered superlattices.

Conclusions

The effect of temperatures on the PtPd nanoparticle superlattices protected with oleic acid and oleylamine was demonstrated with the help of TEM analysis. The PtPd superlattices underwent an irreversible phase transition from an ordered state to a disordered state upon heated to 100 – 110 °C. Proper selection of temperature for heat treatment may help obtain better-ordered superlattices. It is also confirmed that PtPd nanoparticles protected by oleic acid and oleylamine can form hexagon structures when self-assembling into superlattices.

References

A1.   Lin, X.M., C.M. Sorensen, and K.J. Klabunde, 2000 *J. Nanopart. Res.* **V2** 157-64

A2.   Chaki, N.K. and K.P. Vijayamohanan, 2005 *J. Phys. Chem.* **109** 2552-8
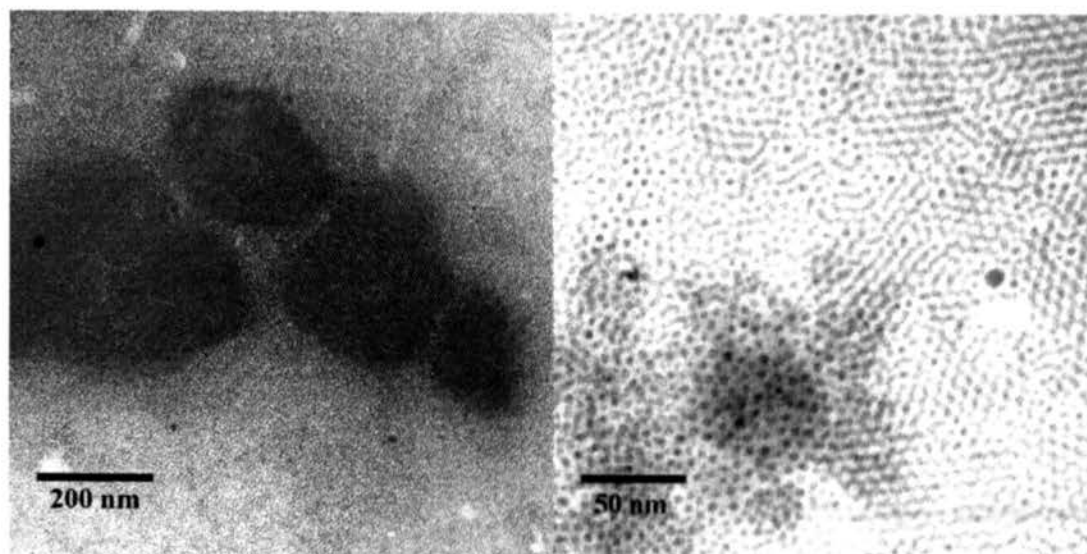
Figure A1. TEM images of PtPd superlattices formed at 23 °C.
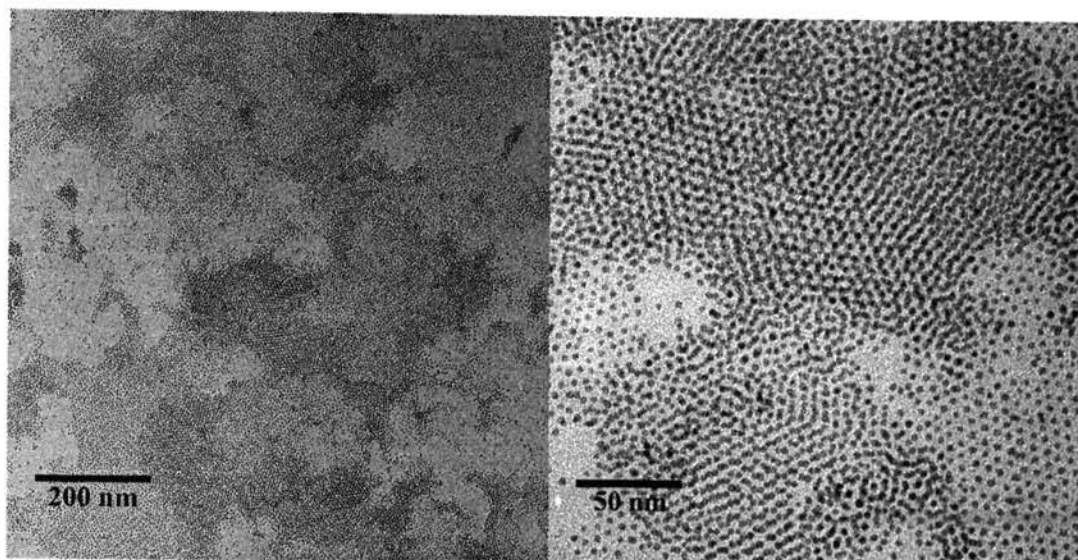
a-1   a-2
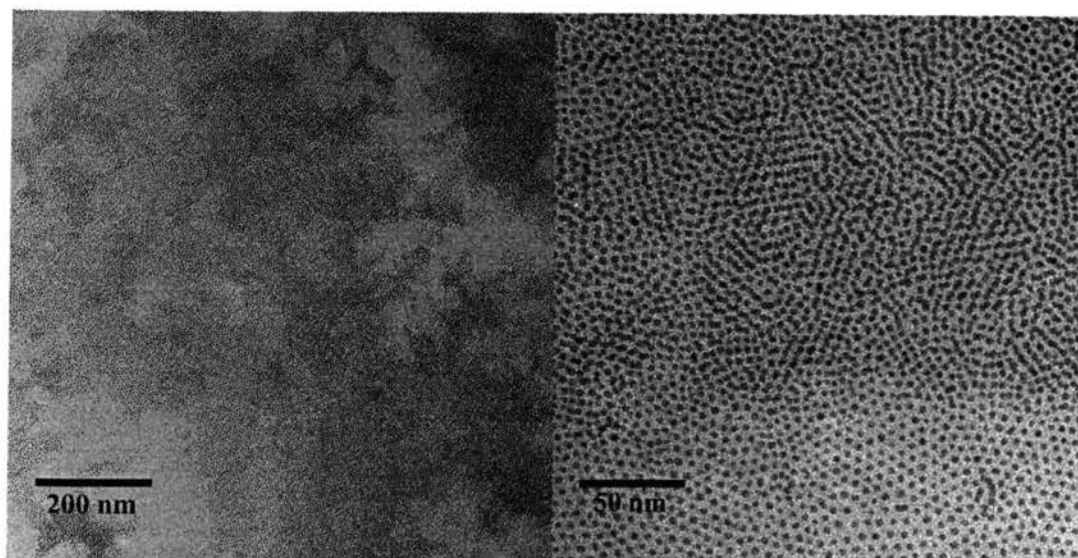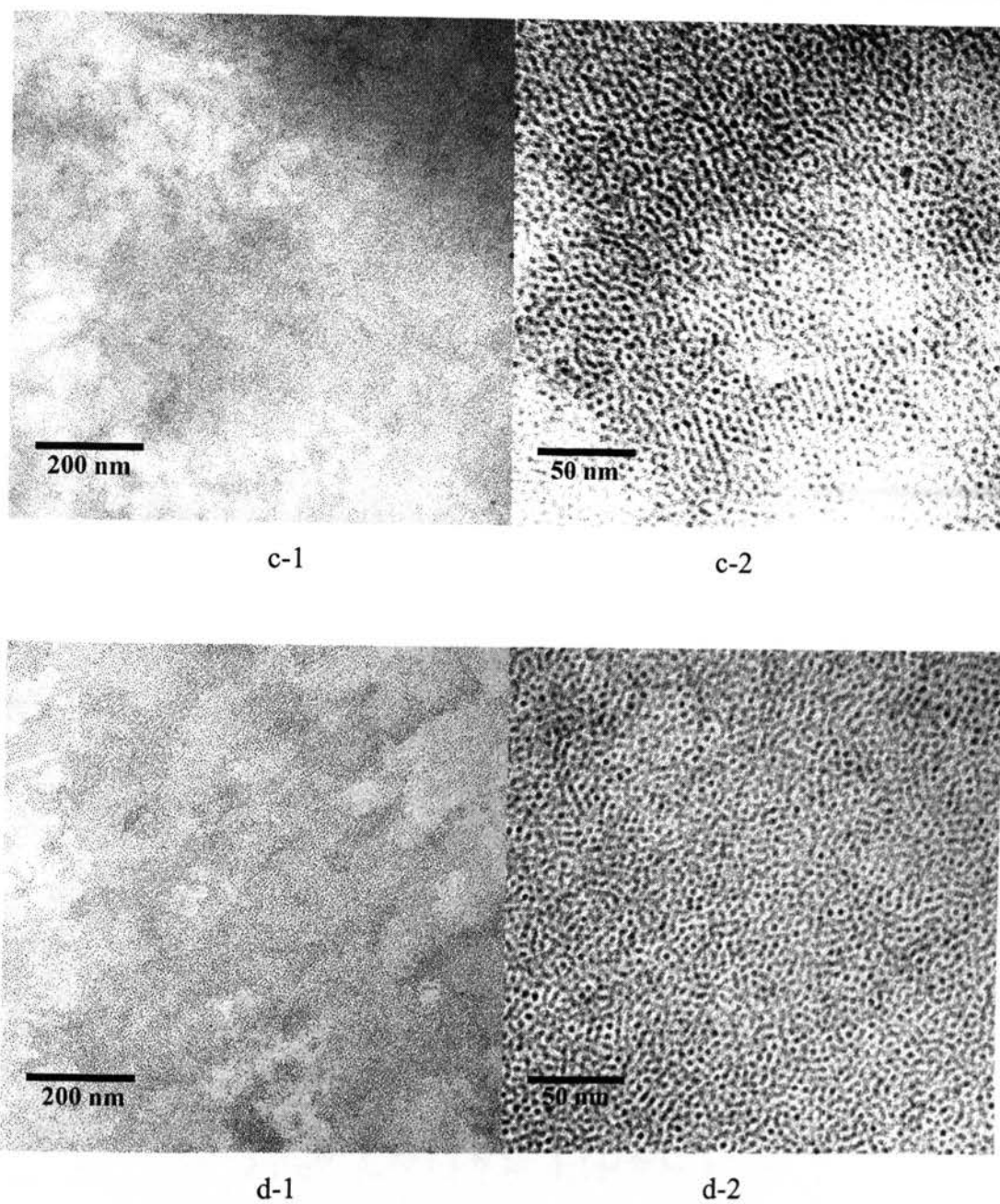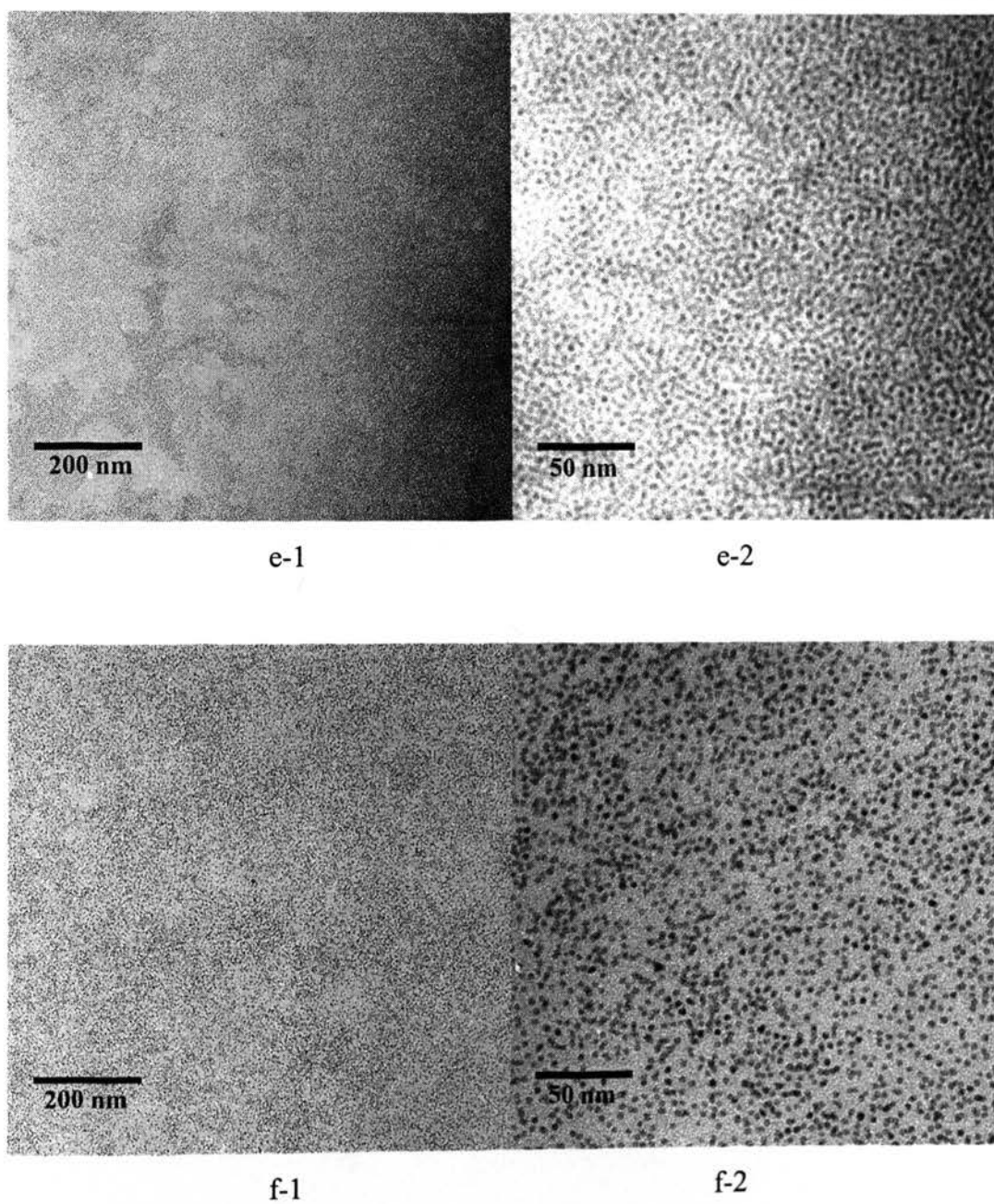
b-1   b-2

Figure A2. TEM images of PtPd superlattices upon heat treatment. PtPd superlattices were treated under different temperatures with the same duration of time; the temperatures from a-h are $60 - 130$ $^{\circ}$C with an increment of 10 $^{\circ}$C.

c-1

c-2

d-1

d-2

Figure A2. TEM images of PtPd superlattices upon heat treatment. PtPd superlattices were treated under different temperatures with the same duration of time; the temperatures from a-h are 60 – 130 °C with an increment of 10 °C. (cont.)
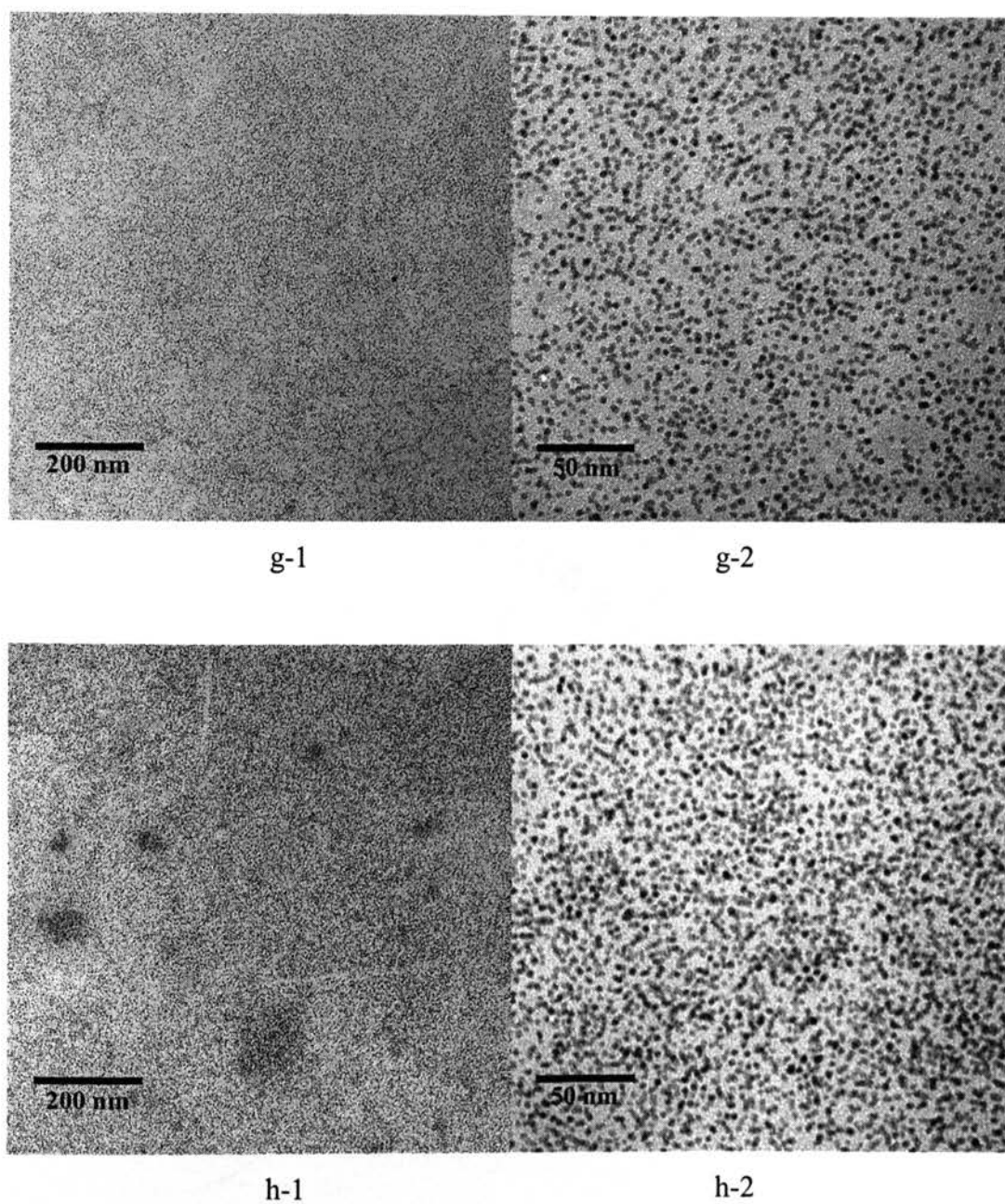
e-1   e-2

f-1   f-2

Figure A2. TEM images of PtPd superlattices upon heat treatment. PtPd superlattices were treated under different temperatures with the same duration of time; the temperatures from a-h are $60 - 130\ ^{o}C$ with an increment of $10\ ^{o}C$. (cont.)

g-1   g-2

h-1   h-2

Figure A2. TEM images of PtPd superlattices upon heat treatment. PtPd superlattices were treated under different temperatures with the same duration of time; the temperatures from a-h are 60 – 130 °C with an increment of 10 °C. (cont.)
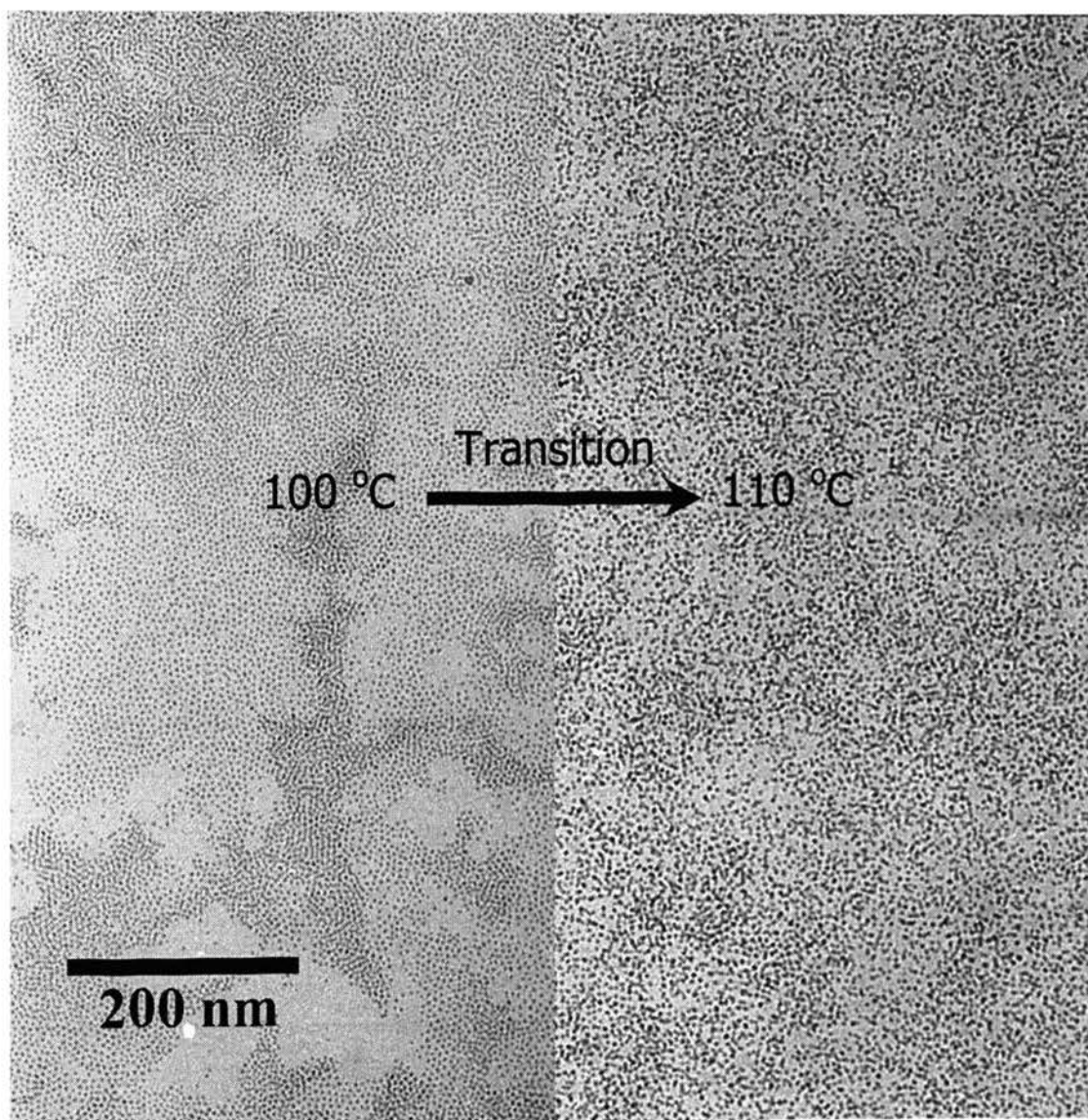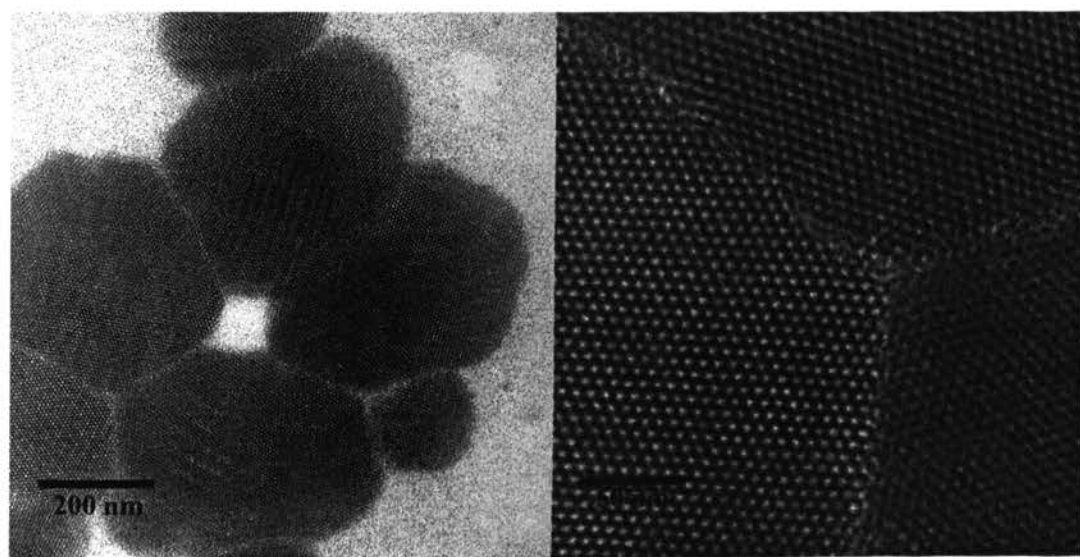
Figure A3. Transition of PtPd superlattices from an ordered structure to a disordered state upon critical temperature.
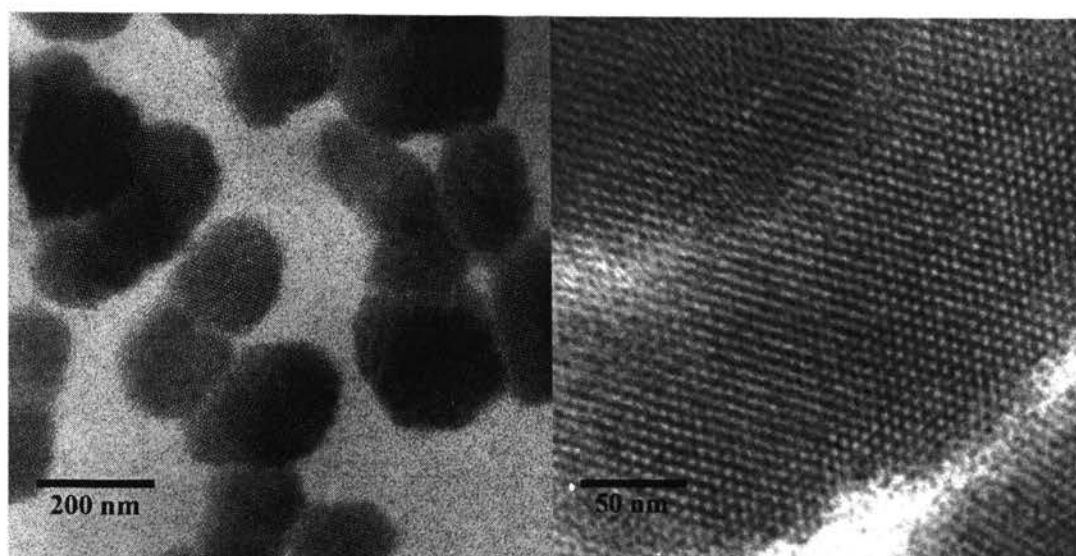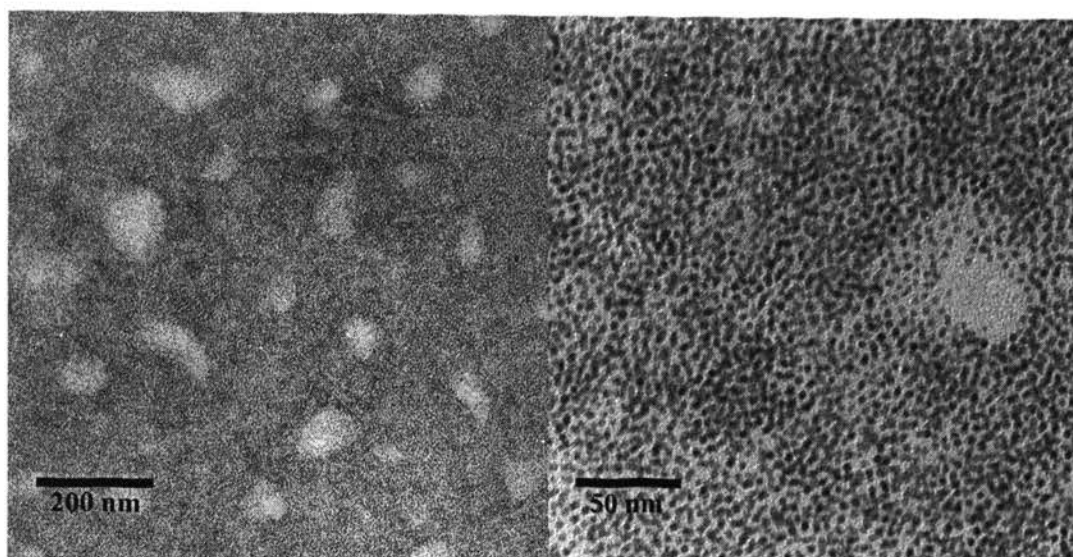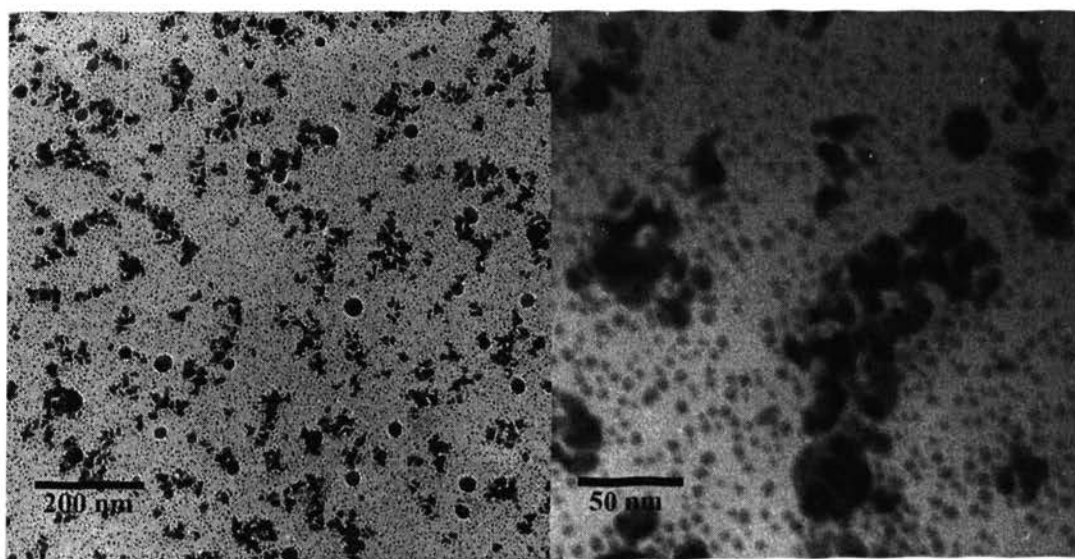
a-1

a-2

b-1

b-2

Figure A4. Temperature-induced restructuring of PtPd superlattices. Sample a is the sample prepared under room temperature 23 °C. b-d are heat treated samples with temperatures 50, 150 and 250 °C, respectively.

c-1   c-2

d-1   d-2

Figure A4. Temperature-induced restructuring of PtPd superlattices. Sample a is the sample prepared under room temperature 23 °C. b-d are heat treated samples with temperatures 50, 150 and 250 °C, respectively. (cont.)
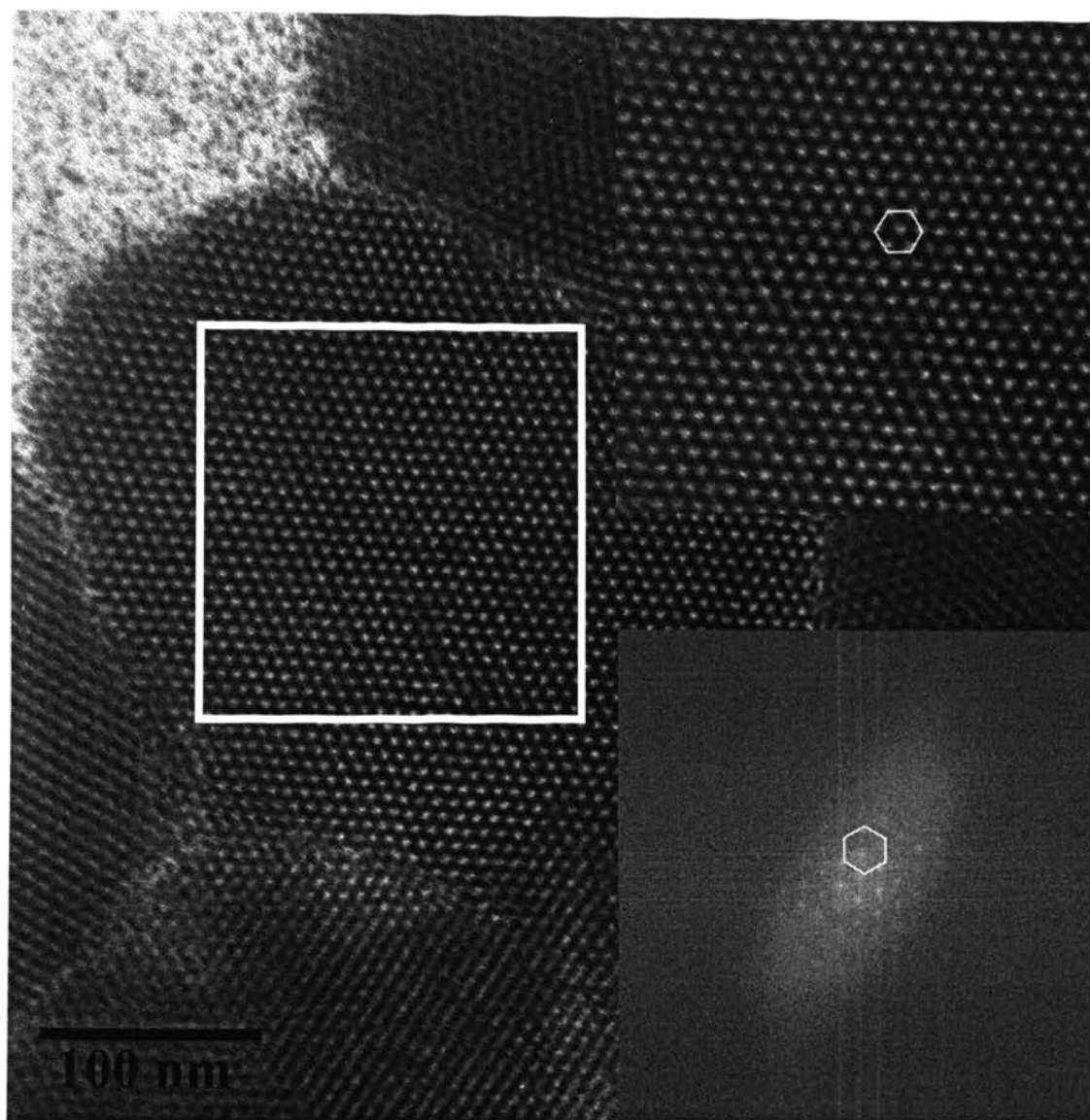
Figure A5. TEM images of 50 °C heat treated PtPd superlattices and the FFT image.

VITA

Mr. Guoqiang Ren was born on September 26th, 1982 in China. He earned a bachelor's degree in Chemical Engineering from the Chemistry and Materials Engineering Department at the Southern Yangtze University (Wuxi, China) in June, 2005. He entered the University of Missouri – Rolla in August, 2005 and obtained his degree of Master of Science in Chemical Engineering from the Department of Chemical & Biological Engineering in August, 2007.